FULL PAPER

ARCH PHARM DPhG
Archiv der Pharmazie

Combining chemical profiles and biological abilities of different extracts from *Tanacetum nitens* (Boiss. & Noë) Grierson using network pharmacology

Stefano Dall'Acqua[1] | Sakina Yagi[2,3] | Stefania Sut[1] | Abdullahi Ibrahim Uba[4] | Sathish Kumar M. Ponniya[5] | Ismail Koyuncu[6] | Kenan Toprak[6] | Mehmet Maruf Balos[7] | Alevcan Kaplan[8] | Uğur Çakılcıoğlu[9] | Gokhan Zengin[10]

[1]Department of Pharmaceutical and Pharmacological Sciences, University of Padova, Padova, Italy

[2]Department of Botany, Faculty of Science, University of Khartoum, Khartoum, Sudan

[3]Le Laboratoire Agronomie et Environnement, Université de Lorraine, INRAE, LAE, Nancy, France

[4]Department of Molecular Biology and Genetics, Istanbul AREL University, Istanbul, Turkey

[5]Department of Bioinformatics, Pondicherry University, Pudhucherry, India

[6]Department of Medical Biochemistry, Faculty of Medicine, Harran University, Sanliurfa, Turkey

[7]Sanlıurfa Provincial Directorate of National Education, Sanlıurfa, Turkey

[8]Sason Vocational School, Batman University, Batman, Turkey

[9]Pertek Sakine Genç Vocational School, Munzur University, Pertek, Tunceli, Turkey

[10]Department of Faculty, Faculty of Science, Selcuk University, Konya, Turkey

Correspondence
Stefano Dall'Acqua, Department of Pharmaceutical and Pharmacological Sciences, University of Padova, via Marzolo 5, 35121 Padova, Italy.
Email: stefano.dallacqua@unipd.it

Funding information
None

Abstract

Tanacetum nitens (Boiss. & Noë) Grierson is an aromatic perennial herb used in Turkish traditional medicine to treat headache, fever, and skin diseases. This study aimed to investigate the chemical composition, antioxidant, enzyme inhibition, and cytotoxic properties of *T. nitens* aerial parts. Organic solvent extracts were prepared by sequential maceration in hexane, dichloromethane, ethyl acetate, and methanol while aqueous extracts were obtained by maceration or infusion. Nuclear magnetic resonance (NMR) and LC-DAD-MS analysis allowed the identification and quantification of different phytoconstituents including parthenolide, tanacetol B, tatridin B, quinic acid derivatives, β-sitosterol, and glycoside derivatives of quercetin and luteolin. The type and amount of these phytochemicals recovered by each solvent were variable and significant enough to impact the biological activities of the plant. Methanolic and aqueous extracts displayed the highest scavenging and ions-reducing properties while the dichloromethane and ethyl acetate extracts exerted the best total antioxidant activity and metal chelating power. Results of enzyme inhibition activity showed that the hexane, ethyl acetate, and dichloromethane extracts had comparable anti-acetylcholinesterase activity and the latter extract revealed the highest anti-butyrylcholinesterase activity. The best α-amylase and α-glucosidase inhibition activities were obtained from the hexane extract. The dichloromethane and ethyl acetate extracts exhibited the highest cytotoxic effect against the prostate carcinoma DU-145 cells. In conclusion, these findings indicated that *T. nitens* can be a promising source of biomolecules with potential therapeutic applications.

KEYWORDS
antioxidant, cytotoxicity, enzyme inhibition, phytoconstituents, *Tanacetum nitens*

1 | INTRODUCTION

The extraordinary diversity of phytoconstituents present in plants makes them a valuable source of potentially useful bioactive natural products. Many of these compounds impart biological activity against several disease-causing agents. Plants are continuously explored to develop pharmaceutical medications for treating diseases like diabetes, cancer, and cardiovascular diseases.[1,2] However, almost 80%–90% of the world's biodiversity is under-explored and can be a promising source of lead molecules that can be efficiently used to treat diseases.[3]

The genus *Tanacetum* (family Asteraceae) is mainly distributed in the Mediterranean region, the two Americas, southwestern and eastern Asia, and in Europe.[4] It comprises about 160 species and some of them like *Tanacetum annuum*, *Tanacetum balsamita*, *Tanacetum indicum*, *Tanacetum nubigenum*, *Tanacetum santolinoides*, *Tanacetum vulgare*, and *Tanacetum parthenium* are used in traditional medicine to treat diabetes, migraine, hypertension, stomach ache, diarrhea, ringworm, and sexually transmitted diseases among others.[5,6] Currently there are increasing interest in *Tanacetum* species due to their effectiveness to cure many diseases and recent studies indicated that some *Tanacetum* species possess antidiabetic,[7] anthelmintic,[8] cholinesterase inhibition,[9] cytotoxic,[10] antioxidant,[11] and antimicrobial[12] activities among others. Essential oils, terpenes, phenols, and steroids were identified in many species, however, the sesquiterpene lactones like germacranolides (parthenolides), eudesmanolides, and guaianolides and flavonoids mainly methylated flavones, flavonols, and agylcones are characteristic compounds of the genus.[13–16]

In Turkey, there are 60 *Tanacetum* species of which 27 are endemic.[17] Among the endemic *Tanacetum* species in Turkey is *Tanacetum nitens* (BOISS. & NOË) GRIERSON (Synonyms; *Chrysanthemum nitens* (BOISS. & NOË) BORNM. and *Pyrethrum nitens* BOISS. & NOË). *T. nitens*, locally called shining tansy, is a perennial herb with finely divided leaves and yellow flowers, found mainly in the inner and south Anatolian regions.[18] It is used as an ornamental plant and in traditional medicine to treat headache, fever, and skin diseases. Chemically, one study on the essential oil composition of the aerial parts was performed and 1,8-cineole (27.57%), α-pinene (4.62%), spathulenol (4.14%), and *trans*-pinocarveol (4.13%) were found to be the major compounds.[19]

However, to the best of our knowledge and based on literature search, research studies on *T. nitens* to valorize their therapeutic potential are not present, and hence, it was hypothesized that *T. nitens* could have a promising pharmacological potential like other species from this genus. This study was undertaken to evaluate the chemical composition, antioxidant, enzyme inhibition, and cytotoxic properties of different extracts from the aerial parts of *T. nitens*. The antioxidant activity was examined by evaluating the capacity of extracts to scavenge radicals, reduce ions, and chelate metals. Enzyme inhibition activity was evaluated against cholinesterase, tyrosinase, α-amylase, and α-glucosidase enzymes while the cytotoxicity was performed against selected cancer cell lines.

2 | RESULTS AND DISCUSSION

2.1 | Total phenolic (TPC) and flavonoid contents (TFC)

The TPC and TFC of different extracts from *T. nitens* aerial parts were determined and results are presented in Table 1. The TPC in different extracts was in the range of 17.21 and 43.49 mg gallic acid equivalents (GAE)/g and in the following descending order; MeOH > aqueous (infusion) > aqueous (maceration) > EtOAc > DCM > hexane. The TFC was ranged between 6.28 and 59.25 mg RE/g and in the following ranking order; MeOH > EtOAc > DCM > aqueous (infusion) > aqueous (maceration) > hexane. Thus, it was clear that polar solvents were found to extract more TPC while polar and less polar organic solvents recovered more TFC. Many, studies showed that the difference in the structure of phenols determines their solubility in solvents.[20,21] The TPC and TFC of many *Tanacetum* species were determined and globally they were found to be rich in phenolics.[22–26]

2.2 | Phytochemical analysis by nuclear magnetic resonance (NMR)-based identification of the main compounds in the extracts

The hexane extract of *T. nitens* once dissolved in deuterated chloroform was subjected to ^{1}H-NMR as well as heteronuclear single quantum coherence (HSQC) and heteronuclear multi bond coherence (HMBC), correlation spectroscopy (COSY) and total correlation spectroscopy (TOCSY) experiments, and all the resonances were mostly ascribed to lipid constituents, as highlighted in the Supporting Information S1: Figures S1–S4. Thus, extraction with hexane is mostly useful to extract the lipids to prepare vegetal material for the further extraction steps.[27]

The dichloromethane and ethyl acetate extracts dissolved in deuterated chloroform showed spectra with larger amounts of signals than the one derived from the hexane extract (Supporting Information S1: Figures S5–S9). Spectra are characterized by signals ascribable to different classes of compounds and some of them were identified using two-dimensional (2D) spectra. The supplementary material shows the

TABLE 1 Total phenolic and flavonoid contents in extracts of *Tanacetum nitens* aerial parts.

Extracts	TPC (mg GAE/g)	TFC (mg RE/g)
Hexane	17.21±0.95[f]	6.28±0.45[f]
Dichloromethane	20.25±0.30[e]	24.72±1.45[c]
Ethyl acetate	25.30±0.84[d]	29.82±0.31[b]
Methanol	43.49±0.97[a]	59.25±0.59[a]
Water (maceration)	37.35±0.43[c]	8.42±0.23[e]
Water (infusion)	39.70±0.53[b]	19.62±0.16[d]

Note: Values are reported as mean ± SD of three parallel measurements. Abbreviations: GAE, gallic acid equivalents; RE, rutin equivalents; TFC, total flavonoid content; TPC, total phenolic content.

^{1}H-NMR, heteronuclear single quantum coherence-distorsionless enhancment by polarization transfer (HSQC-DEPT), HMBC COSY, and TOCSY spectra that allowed the identification of compounds. The extracts obtained with dichloromethane and ethyl acetate are quite similar in terms of detectable signals. Some signals support the presence of sesquiterpene, in particular diagnostic resonances ascribable to parthenolide, the sp^2 methylene (C-13), the CH of the lactone ring (C-6), and the sp^2 CH of position 1 are detected (Supporting Information S1: Figures S10–11). HMBC correlations are observed from the H-13 with the carbonyl lactone (C-12). Other diagnostic positions are related to the presence of the epoxy group that bear the carbon resonances of C-4 and C-5 at δ 61.5 and 51.7. Data are summarized in the Supporting Information S2: Table S1. Furthermore, other signals suggesting the presence of a different sesquiterpene like the sp2 doublets of H-1 and H-15 (δ 5.36 and 5.08–5.19) and the CHO bearing an ester linkage (δ 5.37; 75.2) as well as the quaternary methyl group of an isopropiloxy moiety namely (δ 1.11; 22.7 and 1.23; 28.1). All data are in agreement with the presence of tanacetol B or similar structure.[28] The findings are as summarized in Supporting Information S1: Table S1 and HSQC with the main position of the two sesquiterpenoids is reported in Figure 1.

The aromatic part of the dichloromethane extract shows several signals of low intensity that appear to be aromatic and unsaturated protons. HSQC-DEPT allowed to establish the direct correlation H-C but the HMBC and COSY spectroscopy, due to the low abundance and the large superimposition, did not allow an unequivocal interpretation, so this part of the spectrum was not considered for the lipophilic extracts.

The spectrum of methanol extract is characterized by aliphatic signals supporting the presence of quinic acid derivatives, in particular ester with caffeic moieties (Supporting Information S1: Figures S12–14). chlorogenic acid is one of the most abundant compounds (see resonances in Supporting Information S2: material Table S2). Also, dicaffeoyl-quinic acids are present as supported by multiple minor signals ascribable to H-7′/8′ of the caffeoyl moieties.[29] Sucrose is abundant in the extract and several signals supporting the presence of other sugars are also detected (Supporting Information S1: Figure S14). Signals ascribable to phenolics derivatives are detected in the spectrum region from 5 to 9 ppm. Signals supporting the presence of quercetin glycoside are also detected (Supporting Information S1: Figure S15–S16) and the resonances of position 6 and 8 can be of luteolin-6-C-glycoside as the two singlets at δ 6.59 and 6.51 ascribable to H-6 and H-3 as well as the signals ascribable to position 2′, 6′ and 5′ are observed. The sugar region presents several signals ascribable to anomeric protons of carbohydrate that present in HMBC correlation with aromatic oxygenated carbons suggesting the presence of O-glycosides. Furthermore, anomeric signals ascribable to C-glycosides are observed due to typical chemical shifts (Supporting Information S2: Table S2).[30,31] Signals ascribable to aliphatic CH and deshielded CH$_2$ as well as aromatic can be ascribed to furofuran lignans when compared with the literature and medioresinol and/or trachelogenin were tentatively assigned on the basis of the observed resonances.[32]

Overall, the NMR analysis revealed that the hexane extract was mostly characterized by the presence of lipids while the ethyl acetate and dichloromethane extracts by sesquiterpenoids, mainly parthenolides. Sugars, derivatives of quercetin, luteolin, and caffeic acid as well as lignans were mainly identified in the methanol and water extracts.
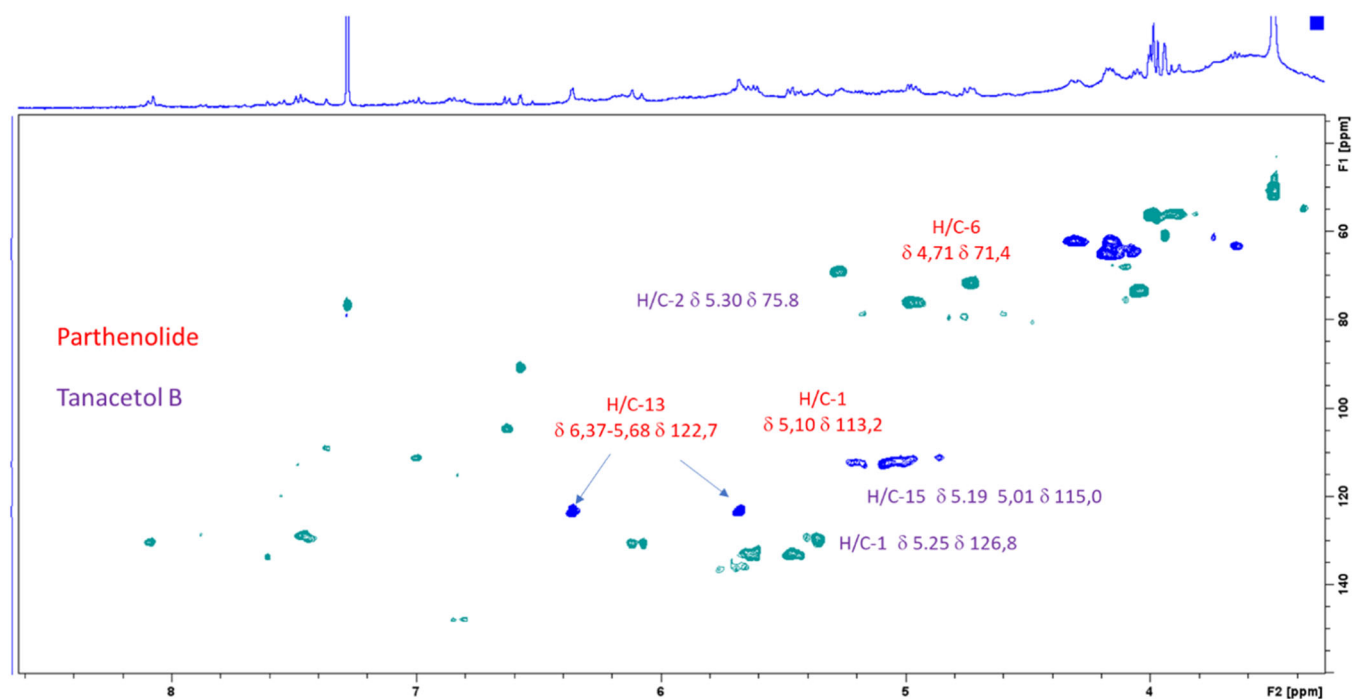
FIGURE 1   HSQC-DEPT of the *Tanacetum nitiens* extracts, parthenolide (red), and tanacetol (purple) main assignments are highlighted.

2.3 | Comprehensive LC-MS analysis of the constituents, data from LC-ESI-QTOF, LC-ESI-MSn and LC-APCI-QQQ to detect and quantify different constituents

The coupling of liquid chromatography with mass spectrometry is one of the more efficient methods for the identification of plant compounds. Different types of mass spectrometry analyser are nowadays available and due to the complex nature of plant extract a combination of different platforms can yield better information and more accurate data. In this regard, the combination of data obtained using ion trap (IT) mass spectrometry that allow multiple-stage mass spectrometry, combined with the quadrupole time of flight (QTOF) was adopted in the present paper. The unique feature of the ion trapping is the opportunity of performing "MS/MS-in-time" experiments, with the possibility of multiple-stage MS/MS fragmentation (MSn)[33] and this is one of the most powerful approaches to collect structural information on chemical species eluted from chromatography. QTOF on the other hand allows us to calculate molecular formula from the accurate MS measurement and allows MS2 analysis after one stage of fragmentation.

Furthermore, it is well known that some compounds can give in electrospray low yields of ionization due to their lipophilic nature, so for the analysis of phytosterols specific APCI-based method was used[34] with the adoption of a triple quadrupole mass spectrometer as a detector.

At first, we compared the information obtained for the different extracts using LC-diode array-MSn and LC-QTOF. In fact, on the basis of the NMR data we observed the presence of different phenolics, so the diode array detector was used to observe the UV spectra of these constituents. Different chromatograms were obtained for the different extracts. In the methanol and water extracts, several peaks presented typical UV spectra of flavonols, caffeic acid derivatives, and simple phenolics were observed. Identification of the compounds was obtained by matching the data obtained from the multiple-stage mass spectrometry that allow to observe the fragmentation of the isolated ion species, the accurate mass and the fragment accurate mass obtained with the QTOF. The IT allows a unique feature because ions are isolated and accumulated and then fragmented using collision-induced dissociation. Process can be repeated several times offering the opportunity to deeply investigate the structure of the analyzed compound. This multiple-stage fragmentation overcome the limits of the QTOF in which the collision cell is one and fragmentation occurred just in one stage, as well as obtained spectra can be partly confused by coeluting species, while in the IT, the parent Ion is isolated and generates a clean series of MSn fragmentation spectra. The compounds were identified by comparing their spectra with the database and literature and finally co-injecting the reference compound when available.

In the methanol extract, significant peaks showed UV absorption with a maximum at 340–350 nm and the typical shape of flavonoids (Table 2). Their HR-MS allowed to establish of molecular formulas, and several isomeric compounds were detected (see Table 2 values of

MS1). Fragmentation of the species in IT was crucial for the structure elucidation. Eight peaks ascribable to flavonoids due to UV spectrum and molecular weight in the MS2 spectra losses of −60, −90, −120, or −180 were observed supporting the presence of C-glycosides moieties.[35] C-glycosides of apigenin and luteolin were identified confirming the data observed in the NMR of the crude extracts. As previously described the IT allowed the observation of the MS2 spectra loss of the first sugar moiety defining in this way the C-6 substituent while in MS3 spectra the loss of the second sugar moiety allowed to identify of the C-8 substituent[36] and the base peaks observed in MS3 spectra after the loss of the second sugar moiety allowed to establish the structure of the flavone aglycones and in particular ions at m/z 353, 369, and 383 were observed supporting the presence of apigenin, luteolin, and chrysoeriol as aglycone.[36]

Also, some O-glycoside derivatives of quercetin and luteolin were identified.[35,37] Quercetin-3-O-glucoside and -glucuronide, luteolin-7-O-glucoside and the methoxy derivative of luteolin nepetin-7-O-glucoside were identified. The position of the glycoside substituents was deduced based on the literature and on the abundance of the ions corresponding to the aglycone moiety as previously described.[38] A second series of peaks present a UV maximum at 320–330 nm and a shape supporting the presence of hydroxycinnamic moiety. For eight peaks were identified, and a first group of three peaks presented a molecular formula corresponding to $C_{16}H_{17}O_9$ and all presenting a main fragment corresponding to a quinic acid moiety supporting that they are all mono caffeoyl quinic acid derivatives. Isomers can be identified due to the different retention times and thanks to the typical fragmentation behavior described by Clifford allowing the identification of three different derivatives. The extract presented an MS2 base peak at m/z 191 and MS3 base peak at m/z 85 supporting the presence of 1-CQA, 3-CQA, and 5-CQA. Further three peaks were identified as dicaffeoyl quinic acids and different isomers were established, observing the MS2 and MS3 fragmentation allowed the identification of 1,3-DCA and 3,5-DCA characterized by the diagnostic ions at m/z 191 as base peak and m/z 179 in MS3 and 4,5-DCA that present base peak ion at m/z 173 in MS3.[39] The remaining caffeoyl hexose and feruloyl quinic acids were deduced from the diagnostic ions observed in MS2. Derivatives of protocatecuic acid were detected as minor constituents. All the phenolics were easily detected in negative ion mode in IT and were analyzed using also positive mode in QTOF. The positive electrospray ionization was the only way to observe and proceed with the identification of the three main sesquiterpenoids namely; parthenolide, tanacetol B, and tatridin B. Parthenolide presented molecular ion [M+H]+ at m/z 249 and intense fragment corresponding to the loss of a water molecule at m/z 231. Tanacetol B presented molecular ion [M+H]+ at m/z 297 and MS2 fragment ion at m/z 237, formed after neutral loss of acetate moiety as well as a specie at m/z 195 derived from the loss of isopropyl group.[40] Tatridin B presented molecular ion [M+H]+ at m/z 265 and fragments at m/z 247 and 229 (Table 2).

APCI source is very effective in the ionization of lipophilic compounds, and it was used on a triple quadrupole mass

TABLE 2 LC-DAD-MS profiles of the extracts (mg/g) of *Tanacetum nitens* aerial parts.

Number	tr	M-H		Fragments	Identification	Hexane	Diclorometane	Ethyl acetate	Metanol	Water (maceration)	Water (Infusion)
1	1.28	191,0555	C7H11O6	173 127 983 85	Quinic acid*	-	0.08	0.10	0.57	0.04	0.13
2	1.68	341,0871	C15H17O9	179 161 143	Caffeoyl hexose	-	0.02	0.02	0.02	0.00	0.01
3	4.07	353,0873	C16H17O9	191 179	3-Caffeoyl quinic acid*	-	0.18	0.20	0.24	0.00	0.42
4	5.09	353,0872	C16H17O9	191 (173 127 85)	1-Caffeoyl quinic acid*	-	0.60	0.62	0.82	0.00	0.10
5	6.08	353,0873	C16H17O9	191 (173 127 85)	5-Caffeoyl quinic acid*	-	0.91	0.88	1.24	0.07	0.11
6	5.46	387,1444	C21H23O7	369 207 209 163	Medioresinol	-	0.08	0.12	0.24	0.01	0.10
7	5.93	387,1444	C21H23O8	369 207 209 163	Medioresinol isomer	-	0.09	0.11	0.17	0.01	0.59
8	6.38	579,1353	C26H27O15	357 327 (299 284 255 213 175)	Luteolin-6-C-hexoside-8-C-pentoside	-	-	-	1.41	0.05	0.00
9	6.96	563,1403	C26H27O14	503 473 443	Shaftoside*	-	-	-	0.39	0.14	0.20
10	7.5	563,1403	C26H27O14	503 473 443	Iso shaftoside	-	0.03	0.03	3.69	1.22	1.78
11	8.68	563,1403	C26H27O14	503 473 443	Neo shaftoside		0.14	0.11	0.60	0.15	0.26
12	7.75	447,0927	C21H19O11	357 327 (299 284 255 213 175)	Luteolin-8-C-glucoside	-	0.36	0.33	2.88	0.08	1.36
13	7.92	447,0927	C21H19O11	357 327 (299 284 255 213 175)	Luteolin-6-C-glucoside (monoorientin)*	-	0.54	0.57	4.58	0.15	1.28
14	11.2	447,0927	C21H19O11	285 241 199 175	Luteolin-7-O-glucoside*	-	0.39	0.45	1.63	0.14	0.54
15	9.14	593,1506	C27H29O15	503 473 413 383	Vicenin II	-	-	0.61	2.16	1.04	1.44
16	11.1	593,1506	C27H29O15	503 473 413 383	Isovitexin-O-glucoside	-	-	0.11	0.52	0.14	0.37
17	9.8	431,0972	C21H19O10	341 311 283 239 181 163	Vitexin (Apigenin-8-C-glucoside)	-	-	0.71	3.78	0.63	0.96
18	10.36	741,3542	C32H37O20	579 459 427 357 327	Luteolin-6-C-glucoside-8-C-arabinoside-O-hexoside	-	-	0.33	0.95	0.00	0.84
19	12.6	609,1455	C27H29O16	301 271 179 151	Rutin	-	-	0.09	0.17	0.00	0.21

(Continues)

TABLE 2   (Continued)

Number	tr	M-H		Fragments	Identification	Hexane	Diclorometane	Ethyl acetate	Metanol	Water (maceration)	Water (Infusion)
20	11.25	461,1083	C22H21O11	341 326 313 298 269 255 225	Scoparin (crisoeriol-8-c-glucoside)	-	0.32	0.41	3.24	0.12	1.15
21	16.25	461,1083	C22H21O11	341 326 313 298 269 255 225	Crisoeriol-6-c-glucoside	-	0.16	0.17	0.71	0.10	0.33
22	15.3	515,119	C25H23O12	191 179 173	3,5-Dicaffeoyl quinic acid*	-	-	-	1.32	0.04	0.42
23	14.8	515,119	C25H23O12	191 179 173	1,3-Dicaffeoyl quinic acid	-	-	-	0.38	0.03	0.16
24	16.8	515,1189	C25H23O12	191 179 173 135	4,5-Dicaffeoyl quinic acid*	-	-	-	0.71	0.02	0.25
25	16.4	491,083	C22H19O13	315 300 179	Isorhamnetin-3-O-glucuronide	-	-	-	0.45	0.00	0.31
26	18.3	491,3083	C23H23O12	314 299 285	Jaceosidin-O-hexoside/tricin-O-hexoside	-	-	-	0.37	-	0.11
27	9.4	463,0873	C21H19O12	301 179	Quercetin-3-O-glucoside*	-	-	-	0.89	0.00	0.28
28	11.3	477,0669	C21H17O13	301 179	Quercetin-3-O-glucuronide	-	-	-	0.71	0.00	0.21
29	14.7	477,0669	C22H21O12	314 300 285 270 257	Nepetin-7-O-glucoside	-	-	-	0.11	0.00	0.03
30	11.3	477,0669	C21H17O13	301 179	Quercetin-O-glucuronide	-	-	-	0.82	0.03	0.30
31	8.93	593,1506	C27H29O15	503 473 413 383	Isovitexin-2"-O-glucoside	-	-	-	0.43	0.00	0.13
32	2.85	315,0723	C13H15O9	153 123	Protocatecuic acid hexoside	-	-	-	0.33	0.00	0.11
33	3.59	315,0723	C13H15O9	153 123	Protocatecuic acid hexoside isomer	-	-	-	0.09	0.00	0.07
34	6.35	367,1033	C17H19O9	193 173 134	3-Feruloyl quinic acid	-	-	-	0.14	0.00	0.06
35	7.28	367,1033	C17H19O10	193 173 134	5-Feruloyl quinic acid	-	-	-	0.06	0.00	0.02
36	8.2	499,1246	C25H23O11	173 161	Feruloyl-coumaroyl quinic acid	-	-	-	0.20	0.00	0.05
37	9.7	529,1381	C26H26O12	367 353	3-Feruloyl-5-caffeoylquinic acid	-	-	-	0.15	0.00	0.07
38	14	529,1381	C26H26O12	367 353	4-Feruloyl-5-caffeoyl quinic acid	-	-	-	0.05	0.00	0.04

TABLE 2 (Continued)

Number	tr	M-H		Fragments	Identification	Hexane	Diclorometane	Ethyl acetate	Metanol	Water (maceration)	Water (Infusion)
39	14.2	529,1381	C26H26O12	367 353	4-Caffeoyl-5-feruloylquinic acid	-	-	-	0.03	0.00	0.03
40	29	329,0661	C17H13O7	314 299 271	Jaceosidin	0.13	0.38	0.40	0.24	0.23	0.11
41	29.3	329,0661	C17H13O7	314 299 271	Cirsiliol	0.09	1.46	1.44	0.22	0.06	0.08
42	29.6	343,0816	C18H15O7	270 242	Eupatilin	0.05	0.14	0.16	0.14	0.00	0.07
					Total	-	6.24		37.26	9.92	14.81
M+H											
43	24.9	249,1409	C15H21O3	231 175	Parthenolide*	0.62	2.33	2.51	0.54	-	0.14
44	27.9	297,2066	C17H29O4	237 195	Tanacetol B	0.19	0.28	0.23	0.05	-	0.01
45	30.2	265,1439	C15H21O4	247 229	Tatridin B	0.23	0.28	0.21	0.01	-	0.00
46	28.3	251,1647	C15H23O3	192 155	Ketopelenolide A or B	0.01	0.17	0.18	0.03	-	0.01
					Total	1.04	3.06	2.98	0.62	-	0.15

Note: Compounds indicated with * were confirmed by authentic standard injection.

TABLE 3 Phytosterols in *Tanacetum nitens* aerial parts.

| | Phytosterols (mg/g) | | | | | |
	Hexane	Dichloromethane	Ethyl acetate	Methanol	Water (maceration)	Water (infusion)
Brassicasterol	0.80	0.53	0.51	0.01	-	-
Campesterol	2.07	0.97	0.89	0.57	-	-
β-Sitosterol	6.29	2.95	2.97	1.58	-	-
Stigmastanol	1.00	0.54	0.55	0.10	-	-

Note: They were confirmed by reference compounds and quantified using authentic standard.

spectrometer to analyze phytosterols. β-sitosterol was the major compound in the hexane and dichloromethane extracts while stigmasterol and sitostanol were present in minor content (Table 3).

The comprehensive analysis on the extracts revealed that the more lipophilic solvents; hexane and dichloromethane can efficiently extract the phytosterol β-sitosterol and sesquiterpene parthenolide. Furthermore, the dichloromethane and ethyl acetate extracted in good amount the previous metabolites and can also efficiently extract the methoxyflavone cirsiliol. A different pattern of phenolic is observed comparing the hexane and dichloromethane and ethyl acetate. In fact, in the hexane fraction no phenolics are detectable while starting from the dichloromethane and moving to the more polar solvents up to methanol we can observe an increase in the number and quantity of phenolic compounds. The most abundant in the methanol extracts are the C-glycoside flavonoids monoorientin, vitexin, and scoparin. Significant differences can be observed considering the water extracts obtained by maceration and infusion.

Most of the phenolics have limited solubility in water and in fact the amount of phenolics in the two different water-based extracts are lower compared with methanol.

2.4 | Anti+oxidant activity

In this study six complementary assays included 2,2-diphenyl-1-picrylhydrazyl (DPPH), 2,2′-azino-bis(3-ethylbenzothiazoline-6-sulfonic acid) (ABTS), cupric reducing antioxidant capacity (CUPRAC), ferric reducing antioxidant power (FRAP), chelating and total antioxidant activity via phosphomolybdenum assay were adopted to evaluate the antioxidant property of *T. nitens* aerial parts and results are depicted in Table 4. Generally, different extracts recovered antioxidant substances with variable mechanisms and capacity. The polar extracts (MeOH and aqueous) revealed significantly ($p < 0.05$) higher radical scavenging activity than other extracts. The MeOH extract (47.52 mg Trolox

TABLE 4 Antioxidant properties of *Tanacetum nitens* aerial parts extracts.

Extracts	DPPH (mg TE/g)	ABTS (mg TE/g)	CUPRAC (mg TE/g)	FRAP (mg TE/g)	Chelating (mg EDTAE/g)	PBD (mmol TE/g)
Hexane	4.13 ± 0.25[e]	10.48 ± 0.15[e]	42.16 ± 0.64[f]	16.98 ± 0.05[f]	34.57 ± 3.06[ab]	1.59 ± 0.08[b]
Dichloromethane	4.57 ± 0.31[e]	20.87 ± 1.49[d]	50.83 ± 0.93[e]	21.02 ± 0.29[e]	35.29 ± 0.11[a]	2.03 ± 0.17[a]
Ethyl acetate	11.41 ± 0.35[d]	28.67 ± 0.72[c]	64.04 ± 0.64[d]	31.62 ± 0.33[d]	23.53 ± 1.25[d]	2.02 ± 0.19[a]
Methanol	47.52 ± 0.04[a]	79.66 ± 0.79[b]	152.61 ± 1.18[a]	69.88 ± 1.05[a]	30.62 ± 0.82[bc]	1.59 ± 0.10[b]
Water (maceration)	31.14 ± 0.75[c]	80.49 ± 0.63[b]	99.60 ± 1.15[c]	50.45 ± 0.27[c]	32.62 ± 0.40[ab]	1.06 ± 0.04[c]
Water (infusion)	45.49 ± 0.60[b]	83.97 ± 0.84[a]	123.12 ± 1.94[b]	62.43 ± 0.73[b]	28.25 ± 1.68[c]	1.09 ± 0.07[c]

Note: Values are reported as mean ± SD of three parallel measurements.

Abbreviations: ABTS, 2,2′-azino-bis(3-ethylbenzothiazoline-6-sulfonic acid; CUPRAC, cupric reducing antioxidant capacity; DPPH, 2,2-diphenyl-1-picrylhydrazyl; EDTAE, EDTA equivalent; FRAP, ferric reducing antioxidant power; MCA, metal chelating activity; PBD, phosphomolybdenum; TE, trolox equivalent.

equivalents [TE]/g) followed respectively by the aqueous extracts obtained by infusion (45.49 mg TE/g) and maceration (31.14 mg TE/g) exerted the highest anti-DPPH activity while aqueous extract obtained by infusion (83.97 mg TE/g) followed by that obtained by maceration and MeOH extract (80.49 and 79.66 mg TE/g) exerted the highest anti-ABTS activity. The same pattern was observed for the Cu^{++} and Fe^{+++} ions reducing capacity of extracts where the highest significant ($p < 0.05$) activity was displayed respectively by the MeOH (CUPRAC = 152.61; FRAP = 69.88 mg TE/g), aqueous (infusion) (CUPRAC = 123.12; FRAP = 62.43 mg TE/g) and aqueous (maceration) (CUPRAC = 99.60; FRAP = 50.45 mg TE/g) extracts. On the other hand, the DCM extract (35.29 mg EDTA equivalent (EDTAE)/g) showed significantly ($p < 0.05$) the highest chelating power followed by the hexane and aqueous (maceration) extracts (34.57 and 32.62 mg EDTAE/g, $p \geq 0.05$). Furthermore, the less polar extracts (DCM and EtOAc) exerted significantly ($p < 0.05$) higher total antioxidant activity (2.03 and 2.02 mmol TE/g) than other extracts (≤ 1.59 mmol TE/g). Overall, it was noted that phytoconstituents with the highest antiradical and ions reducing capacity were mainly recovered from the MeOH and aqueous extracts while those with the best total antioxidant properties were mainly accumulated in the less polar extracts (DCM and EtOAc) extracts indicating that *T. nitens* contained antioxidant molecules with variable mechanisms of action. Previous studies showed a positive correlation between the antioxidant of extracts to their TPC.[22–26] The antioxidant activity of phenolics depends on their structure, particularly the number and position of hydroxyl groups in the aromatic rings.[41] Compounds like luteolin glucosides,[42] vitexin,[43] iso shaftoside,[44] 3,5 dicaffeoyl quinic and 5 caffeoyl quinic acids,[45] which were relatively in higher abundance in the polar extracts, could effectively participated in the antioxidant activity. Moreover, these results supported previous studies that highlighted the potential of *Tanacetum* species as a promising source of antioxidant substances.[22–26]

2.5 | Enzyme inhibition activity

Enzymes play a vital role in a wide range of physiological reactions and abnormal enzymatic activity leads to a diverse range of diseases like

diabetes, hyperpigmentation, and Alzheimer's diseases.[46] Thus, the identification of inhibitors of many clinically relevant enzymes has been considered as a promising strategy to treat many diseases.[47] In the present study, extracts of *T. nitens* aerial parts were evaluated for their capacity to inhibit the acetylcholinesterase (AchE), butyrylcholinesterase (BchE), tyrosinase (Tyr), *α*-amylase and *α*-glucosidase enzymes. Results are shown in Table 5. The less and nonpolar extracts showed higher cholinestrase inhibition activity when compared with that exerted by the polar extracts. The highest value against the acetylcholinesterase (AChE) was recorded from the DCM extract (2.54 mg galantamine equivalent [GALAE]/g) followed by EtOAc (2.17 mg GALAE/g) and hexane (1.96 mg GALAE/g) extracts, respectively. The hexane, DCM and EtOAc extracts displayed comparable anti-butyrylcholinesterase (BChE) activity (3.93–4.29 mg GALAE/g, $p \geq 0.05$). These results supported the cholinestrase inhibition property of *Tanacetum* species. In a screening study of 36 extracts from the leaf, stem, and flower of 17 *Tanacetum* species growing in Turkey for their AChE and BChE inhibition activity at 100 μg/mL, it was found that five extracts exerted anti-AChE activity > 90% and eight extracts had activity between 80% and 90% with the leaf extract of *T. argenteum* subsp. *flabellifolium* had the highest AChE inhibition (96.68%), while the best BChE-inhibiting effect (63.81%) was recorded by the stem extract of *T. argyrophyllum* subsp. *argyrophyllum*.[48] Furthermore, they observed that the major compound of these species, parthenolide, exerted a moderate inhibition against AChE (25.46%) and BChE (14.98%) and thus they suggested a synergistical effect of parthenolide together with other substances present in extracts was responsible of the observed activity.[48]

All extracts revealed considerable anti-Tyr activity in the range of 35.76 and 64.84 mg KAE/g with the highest and lowest values were recorded by the MeOH and aqueous extracts respectively. The anti-Tyr activity could be associated with the richness of these extracts in flavonoids.[49] Comparing these results with those obtained from other *Tanacetum* species showed that the anti-Tyr activity of organic solvents extracts was higher than that recorded by Gevrenova et al.[24] on hydromethanolic (80%) extracts of *T. balsamita* roots, leaves, and flowers tips (45.49–54.65 mg KAE/g) and by Ak et al.[22] on different extracts of *T. vulgare* flowers, stems and aerial parts (22.26–32.93 mg KAE/g).

TABLE 5 Enzyme inhibitory properties of *Tanacetum nitens* aerial parts extracts.

Extracts	AChE (mg GALAE/g)	BChE (mg GALAE/g)	Tyrosinase (mg KAE/g)	Amylase (mmol ACAE/g)	Glucosidase (mmol ACAE/g)
Hexane	1.96 ± 0.10^b	3.93 ± 0.18^a	58.54 ± 0.76^c	0.60 ± 0.01^a	0.61 ± 0.01^a
Dichloromethane	2.54 ± 0.27^a	4.26 ± 0.54^a	61.28 ± 0.38^b	0.47 ± 0.01^c	0.55 ± 0.02^b
Ethyl acetate	2.17 ± 0.07^{ab}	4.29 ± 0.17^a	59.77 ± 0.28^{bc}	0.54 ± 0.01^b	0.33 ± 0.05^c
Methanol	1.06 ± 0.19^c	1.18 ± 0.38^b	64.84 ± 0.31^a	0.35 ± 0.01^d	na
Water (maceration)	na	0.64 ± 0.05^{bc}	35.76 ± 0.65^e	0.18 ± 0.01^e	na
Water (infusion)	na	0.20 ± 0.03^c	42.21 ± 1.85^d	0.08 ± 0.01^f	na

Note: Values are reported as mean±SD of three parallel measurements.

Abbreviations: ACAE, acarbose equivalent; AChE, acetylcholinesterase; BChE, butyrylcholinesterase; GALAE, galantamine equivalent; KAE, kojic acid equivalent; na, not active.

TABLE 6 Cytotoxic effect of *Tanacetum nitens* aerial parts extracts.

Cell lines	IC$_{50}$ (µg/mL)					
	Hexane	Dichloromethane	Ethyl acetate	Methanol	Water (maceration)	Water (infusion)
HeLa	109.5	51.18	37.41	52.48	60.87	63.82
HT-29	45.55	29.99	31.2	55.62	98.28	52.29
HGC-27	90.3	56.5	54.3	112.3	54.3	88.5
MCF-7	96.5	65.4	88.4	98.4	140.3	78.4
A549	112.3	36.5	45.6	78.6	65.4	100.3
MDA-MB-231	99.21	60.02	87.17	83.43	115.3	100.4
DU-145	111.3	14.1	14.57	115.5	68.23	117.2

Concerning the enzyme inhibition activity of extracts against the two enzymes associated with diabetes, it was observed that the non and less-polar extracts exerted the best α-amylase (0.47–0.60 mmol acarbose equivalent [ACAE]/g) and α-glucosidase (0.33–0.61 mmol ACAE/g) inhibition activity with highest significant ($p < 0.05$) values recorded from the hexane extract. Polar extracts were either inactive or displayed weak activity against these two enzymes. The inhibition property of *Tanacetum* species against α-amylase and α-glucosidase was variable. For example, the essential oil from *T. praeteritum* subsp. *praeteritum* aerial parts inhibited the α-amylase with IC$_{50}$ value 0.89 mg/mL.[50] Ak et al.[22] found that different extracts of *T. vulgare* flowers, stems and aerial parts displayed a potent α-glucosidase inhibition activity (3.57–10.77 mmol ACAE/g). In a recent study, Gevrenova et al.[24] found that roots hydromethanolic extract of *T. balsamita* revealed high α-amylase and α-glucosidase inhibition activity (IC$_{50}$ value 0.43 and 0.71 mmol ACAE/g respectively) and the activity was attributed to the presence of flavonoids and acylquinic acids. In another study, the α-amylase inhibition activity (356.9 mg ACAE/g) of EtOAc extract from *T. haussknechtii* capitula was attributed to the presence of

caffeoylquinic acid derivatives.[25] However, in the present study, the best activity against these two enzymes was recorded from the hexane extract which is devoid of the aforementioned compounds and thus, suggesting that the substances responsible of antidiabetic activity in *Tanacetum* species varied according to species, studied organ, and type of extract. A previous study demonstrated that β-sitosterol attenuate insulin resistance and could play a potential role in diabetes management.[51] It could be speculated that β-sitosterol which present in high content in hexane extract may participated in this activity.

2.6 | Cytotoxicity

Cancer is a disease characterized by aberrant cell proliferation and invasiveness of abnormal cells to neighboring tissues and it is considered as one of the top leading causes of death in the world.[52] In the present study, the cytotoxic effect of different extracts from the aerial parts of *T. nitens* was evaluated against seven cancer cells namely; HeLa, HT-29, HGC-27, MCF-7, A549, MDA-MB-231, and DU-145 and results are presented in Table 6. Interestingly, the DCM extract displayed the

highest cytotoxic effect against five cancer cells with cytotoxic effect, represented as IC_{50} values, against different lines in the following order; DU-145 (14.1 µg/mL) > HT-29 (29.99 µg/mL) > A549 (36.5 µg/mL) > MDA-MB-231 (60.02 µg/mL) > MCF-7 (65.4 µg/mL). The EtOAc extract also exerted remarkable cytotoxicity against the prostate carcinoma DU-145 cells with IC_{50} value (14.57 µg/mL) comparable to that recorded by the DMC extract. It also exerted the highest cytotoxicity against HeLa (IC_{50} 37.41 µg/mL) and HGC-27 (IC_{50} 54.3 µg/mL) cell lines. The aqueous extract obtained by maceration revealed the same cytotoxic effect as that exerted by the EtOAc extract against HGC-27 (54.3 µg/mL) cell line. All other extracts were less effective against the tested cancer cell lines. However, it was observed that both the DCM and EtOAc extracts were dominated by relatively high accumulation of parthenolide and cirsiliol. In fact, the anticancer activity of these two compounds was previously illustrated. Parthenolide, which was firstly isolated from *T. parthenium*, was shown to induce the death of many cancer cell like prostate cancer CD44+, breast cancer stem-like cells and chronic myelogenous leukemia (CML) via the inhibition of nuclear transcription factor-kappa B (NF-κB), or inhibitory effects on inflammasome activity via NLRP3 and signal transducer and activator of transcription (STAT 1 and STAT3).[53,54] Cirsiliol was also proven to inhibit colon cancer cell proliferation by targeting the STAT3.[55] Furthermore, the cytotoxicity of some *Tanacetum* species was previously determined. For example, hydroethanolic extract and essential oil of *T. vulgare* aerial parts were shown to possess a cytotoxic effect against MCF-7 (IC_{50} 286.6 µg/mL) and colon adenocarcinoma cell lines DLD-I (IC_{50} 105 µg/mL) respectively.[10,56] Five sesquiterpenes isolated from the flower possessed cytotoxic effect against A549 and hamster lung fibroblast cells (V79379A) (IC_{50} 15.3 – 49.4 µg/mL).[57] In another study, chloroform extracts from *T. vulgar*, *T. macrophyllum*, and *T. corymbosum* aerial parts were found to reveal cytotoxic effect against A549 and HeLa cells in a dose-dependent manner.[58] Thus, *Tanacetum* species can be considered as promising source of anticancer molecules.

2.7 | Molecular modeling results

The molecular docking analysis performed here is to get insights into the binding mode and interaction patterns of the most abundant bioactive compounds in the extracts of *T. nitens*. The calculated binding energy revealed compounds with the highest binding propensity (Figure 2). For example, vicenin-II, luteolin-8-C-glucoside, luteolin-6-C-glucoside, and rutin were predicted to have good binding strength against all the studied target proteins. In particular, vicenin-II, via its multiple hydroxyl groups, bound to AChE by forming H-bonds with Tyr72, Asp75, Se293, Arg296, and Tyr341; and a charged attraction with Arg296. In addition, a π–π stacking interaction with Trp286 and several van der Waals interactions reinforced the binding (Figure 3a). Phe295, which formed hydrophobic contact, is considered as one of the important constituents of the AChE active site which participates in the formation of the acyl pocket subsite.[59] The key interactions between vicenin-II and BChE are H-bonds with Asn289 and His428, metal–acceptor interaction with the active site Zn^{2+} metal ion, π–π stacking interaction with Phe329, and multiple hydrophobic contacts with residues in the catalytic channel of the enzymes. Of the residues involved in the hydrophobic interaction was Ala328 (Figure 3b)—a catalytically essential residue whose mutation affects the activity of BChE.[60] Similarly, the key interactions between amylase and vicenin-II were H-bonds between the hydroxyl groups of the ligand and His30, Thr163, and Asp300, as well as a few hydrophobic contacts (Figure 3c). The same compound occupied the catalytic channel of glucosidase and formed H-bonds with the backbone of Leu41, the sidechain of Asp163, Arg173, and few other contacts (Figure 3c). Therefore, the shape of vicenin-II coupled with its multiple hydroxyl groups allows the compound to bind strongly to these targets, thereby potentially inhibiting their activity.

Furthermore, to predict their anticancer potential, the dominant bioactive compounds were also docked into the active site of cancer target proteins: FGFR2,[19] VEGFR2,[41] and PD-L1.[1] Luteolin-6-C-glucoside was accompanied in the binding pocket of FGR2 via a charged
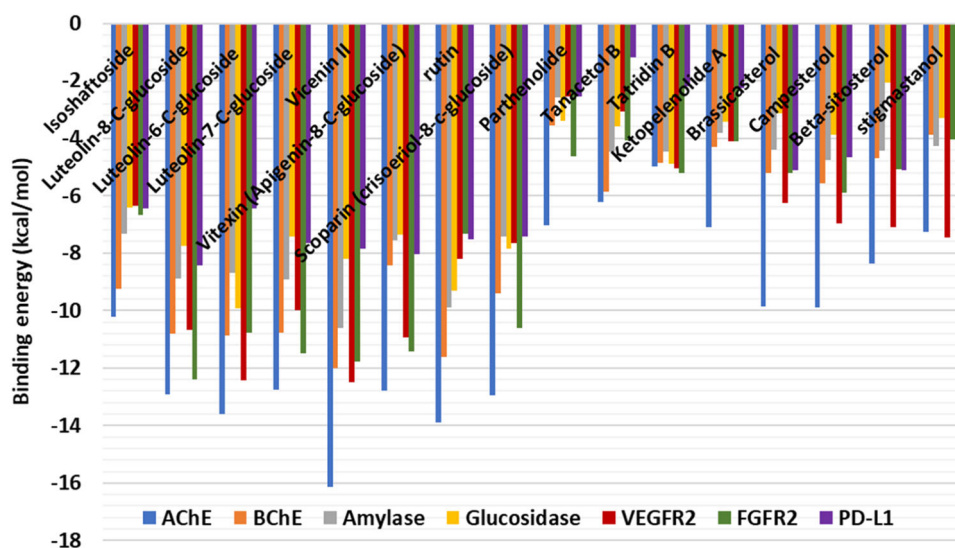

FIGURE 2 Docking score of the most abundant bioactive compounds in the extracts of *Tanacetum nitens*.
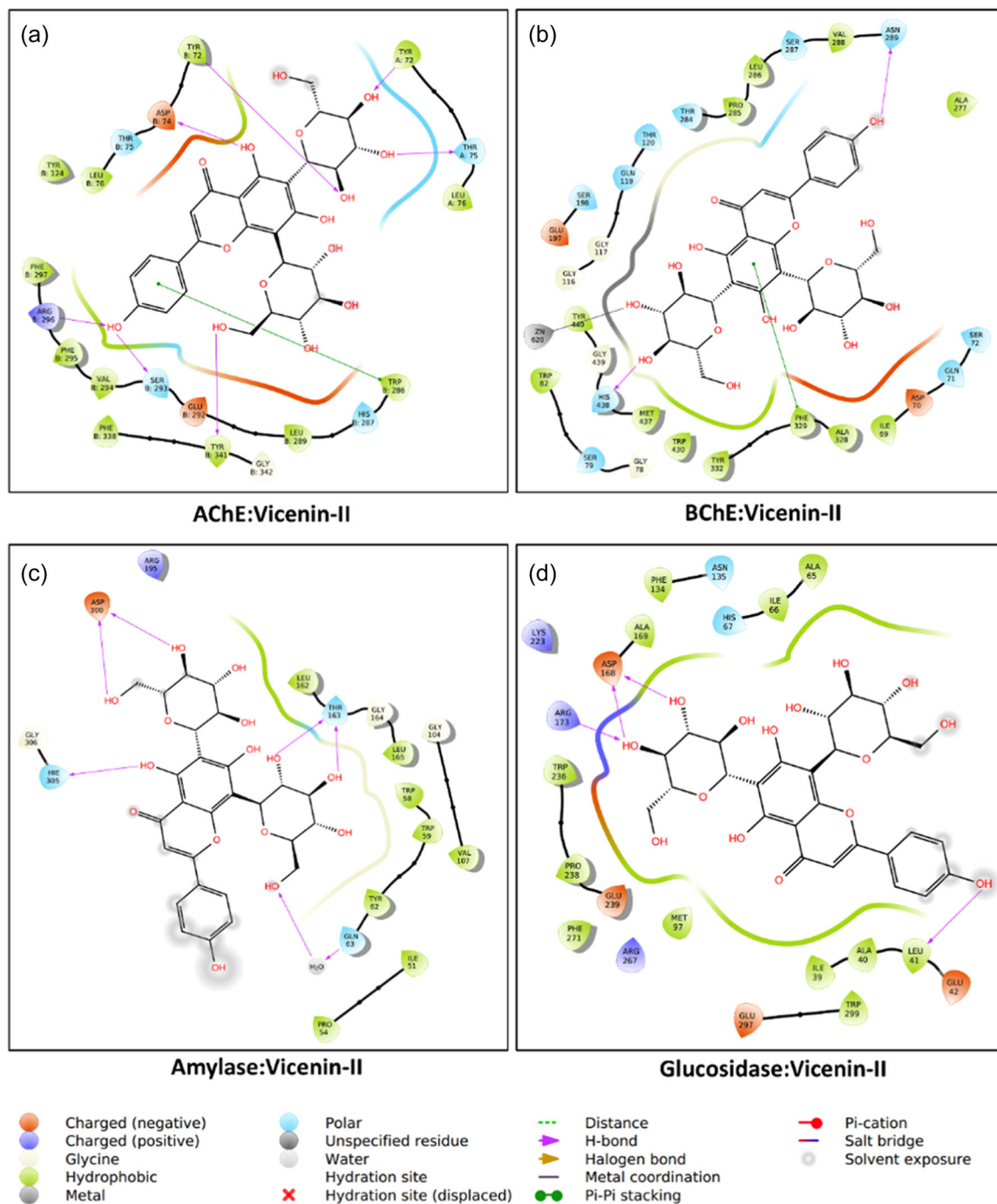
FIGURE 3 Interaction between vicenin-II from *Tanacetum nitens* and: (a) acetylcholinesterase (AChE), (b) butyrylcholinesterase (BChE), (c) amylase, and (d) glucosidase.

interaction with Lys517; H-bonds with the backbone of Phe492 and ala567, and the sidechain of Cys491 and Asp644. Other contributors include a few hydrophobic contacts and van der Waals interactions (Figure 4a). It is interesting to note that a similar compound luteolin-8-C-glucoside interacted with VEGFR2 mainly via H-bonds with the backbone of Leu840 and the sidechain of Glu917, Cys919, and Asn923; a charged interaction with Arg105; and a few hydrophobic and van der Waals interactions with amino acid residues in the tunnel

(Figure 4b). Finally, the same compound demonstrated potential PDL-1 inhibition by forming multiple H-bonds with the backbone of Phe19 and the sidechain of Tyr20, Asp61, Asn63, and Gln66; π–π stacking interactions with Tyr56 and Tyr123, as well as few hydrophobic and van der Waals interactions (Figure 4c). Taken together, H-bonds are the key interactions by which the most abundant compounds in the extracts of *T. nitens* such as vicenin-II, luteolin-6-C-glucoside, and luteolin-8-C-glucoside potentially block the activity of the studied proteins.
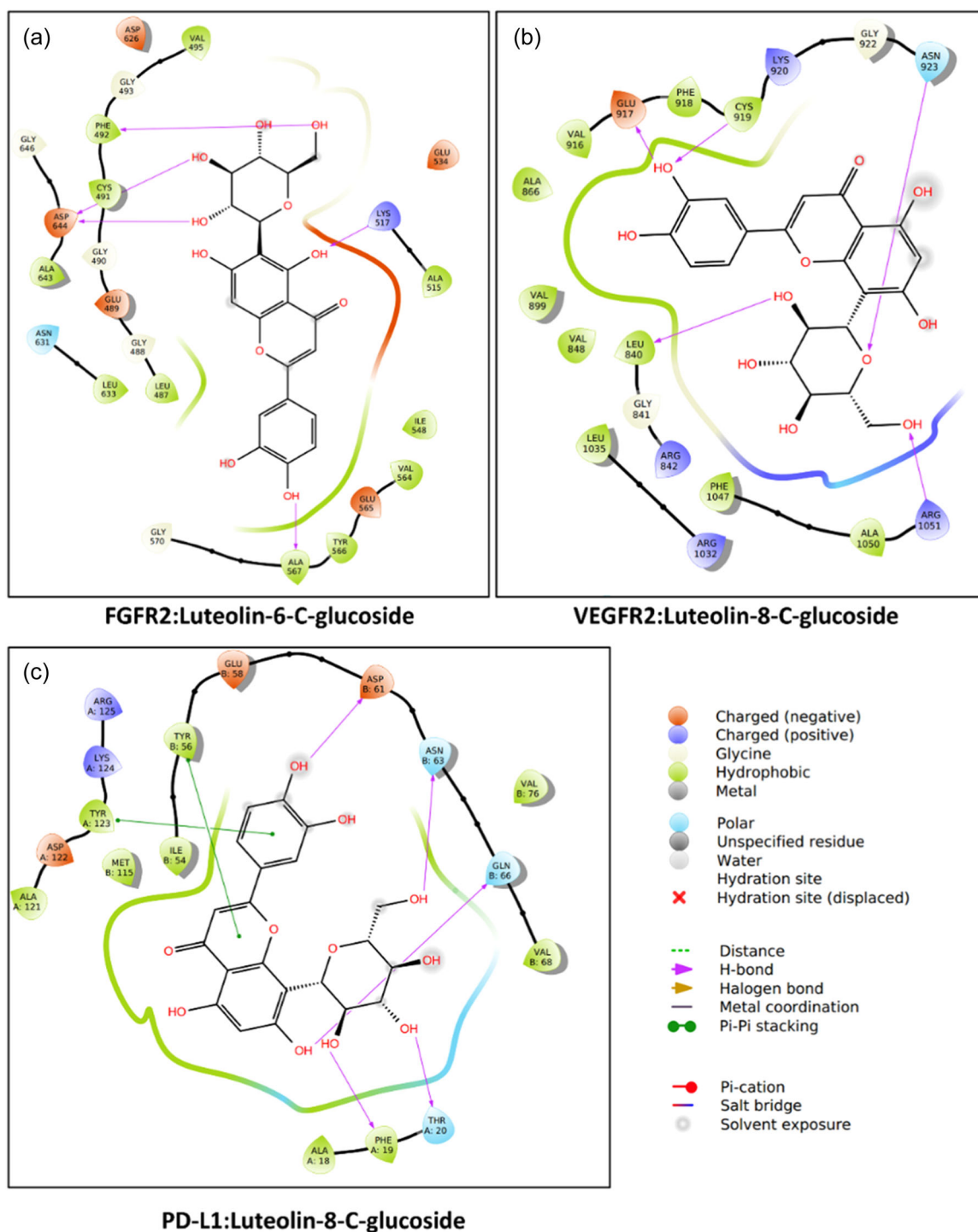
FIGURE 4 Interaction of the most abundant bioactive compounds from *Tanacetum nitens* with some cancer target proteins: (a) VEGFR-2 and luteolin-8-C-glucoside, (b) FGFR2 and luteolin-6-C-glucoside, and (c) PD-L1/PD-1 and luteolin-8-C-glucoside.

2.8 | Network pharmacology

2.8.1 | Target identification and compound-target network

In our study, Swiss Target Prediction was employed to forecast targets for 45 compounds of *T. nitens*, with a screening threshold probability score of ≥0.1, yielding a total of 252 unique targets. Subsequently, targets associated with rheumatoid arthritis (RA), initially numbering 686 from the Open Target Platform, were refined to 43 targets with an overall association score >0.5 for subsequent analysis. A Venn diagram created using Venny 2.1.0 revealed 14 overlapping targets shared between *T. nitens* and RA (Figure 5). The compound-target network was constructed using an attributed
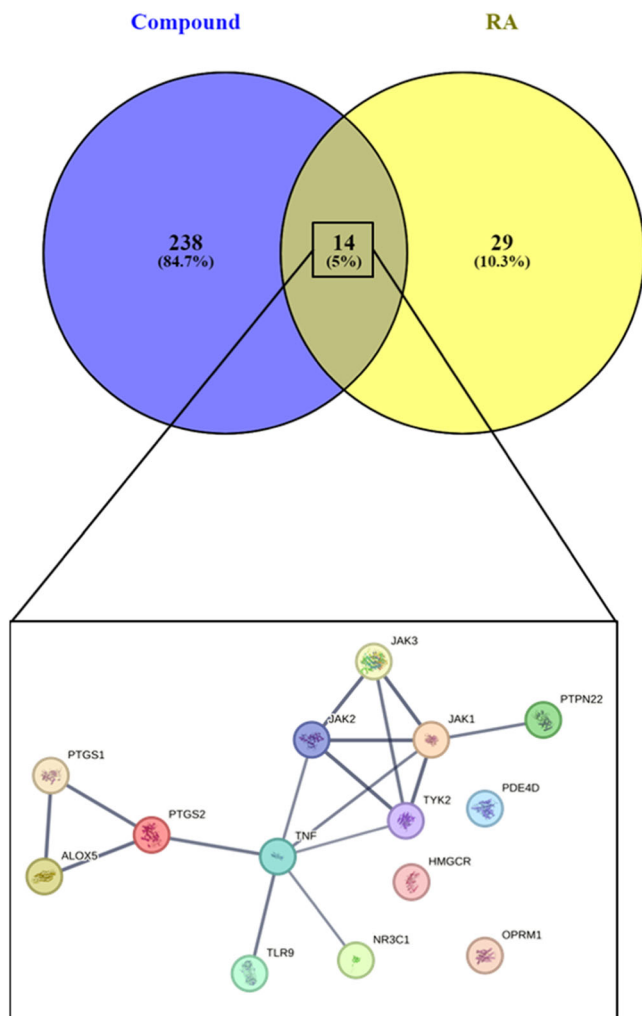
FIGURE 5 The Venn diagram illustrates the overlap of 14 targets associated with *Tanacetum nitens* and rheumatoid arthritis (RA). Subsequently, a protein–protein interaction network was constructed, highlighting the common targets.

circular layout for compounds and an attributed grid layout for targets. Compounds, targets, and common targets were represented as hexagonal, rectangular, and downward arrow nodes, respectively (Figure 2). The network demonstrated a highly interconnected structure, comprising 299 nodes and 803 edges, with an average of 5.371 neighbors per node and a density of 0.009. The characteristic path length between any two nodes was found to be 1.204.

2.8.2 | Protein–protein interactions

The protein–protein interaction network delineates functional and physical interactions, characterized by a high-confidence threshold exceeding 0.7. In Figure 2, a visual representation of the network highlights 14 common targets. This depiction underscores significant connectivity among these proteins, accentuating their functional and biological interdependence. The network analyzed in Cytoscape

comprises 11 nodes and 16 edges, as depicted in Figure 6. With an average connectivity of four neighbors per node, the network demonstrates significant interconnectivity. Moreover, it exhibits a density of 0.291 and a characteristic path length of 2.145. Notably, it has a diameter of 4, representing the shortest distance between the most distant nodes, indicating a connected loop formation conducive to circular interactions. The nodes exhibit clustering, with a clustering coefficient of 0.518. The top five hub genes were TNF, JAK1, JAK2, TYK2, and PTGS2.

2.8.3 | Gene ontology and Kyoto Encyclopedia of Genes and Genomes (KEGG) pathway analysis

The common targets were taken for a comprehensive analysis to elucidate their involvement in biological processes, cellular components, molecular functions, and pathways via gene ontology and KEGG pathway assessment. A graphical representation in the form of a bar plot illustrates the gene ontology of the 14 targeted proteins, highlighting the top 20 biological processes, molecular functions, and cellular components (Figure 7). The chromosomal location of common genes is depicted in a genome plot through a bar graph. Figure 8 showcases bar plots representing the top 20 pathways. *T. nitens* compounds were involved in inflammation-related pathways, notably the Janus kinase/signal transducers and activators of transcription (JAK-STAT) signaling pathway, Th1 and Th2 cell differentiation, and Th17 cell differentiation. Furthermore, hub genes identified for *T. nitens* compounds within the JAK-STAT signaling pathway comprise JAK1, JAK2, and TYK2, as depicted in Figure 9.

Tanacetum species have a long history of utilization in traditional medicine. for conditions like rheumatism, anemia, hypercholesterolemia, and kidney weakness.[19] RA is characterized by chronic inflammation affecting numerous joints in the body. This condition leads to swelling and thickening of the synovium, typically a thin membrane lining the joints, due to the infiltration of both immune and nonimmune cells. This process is driven by elevated levels of chemokines and adhesion proteins.[21] Additionally, high levels of proinflammatory cytokines and growth factors, mainly produced by cells within the synovium, contribute to joint damage by eroding the cartilage and bones. The activation of the Janus kinase/signal transducers and activators of transcription (JAK/STAT) signaling pathway by proinflammatory cytokines is a pivotal contributor to the onset and advancement of rheumatoid arthritis.[61]

The human JAK family encompasses four members: JAK1, JAK2, JAK3, and TYK2, whereas theJAK1 and JAK2 were implicated to type II interferon (interferon-gamma) signaling, while JAK1 and TYK2 were associated with type I interferon signaling (Stoiber et al.[48]). The JAK-STAT signaling mechanism is crucial for transmitting signals from specific type I and type II cytokine receptors which lacks inherent kinase activity, and depend on JAKs to phosphorylate downstream proteins following ligand binding. Upon receptor activation, JAKs interact with the cell membrane, leading to their autophosphorylation
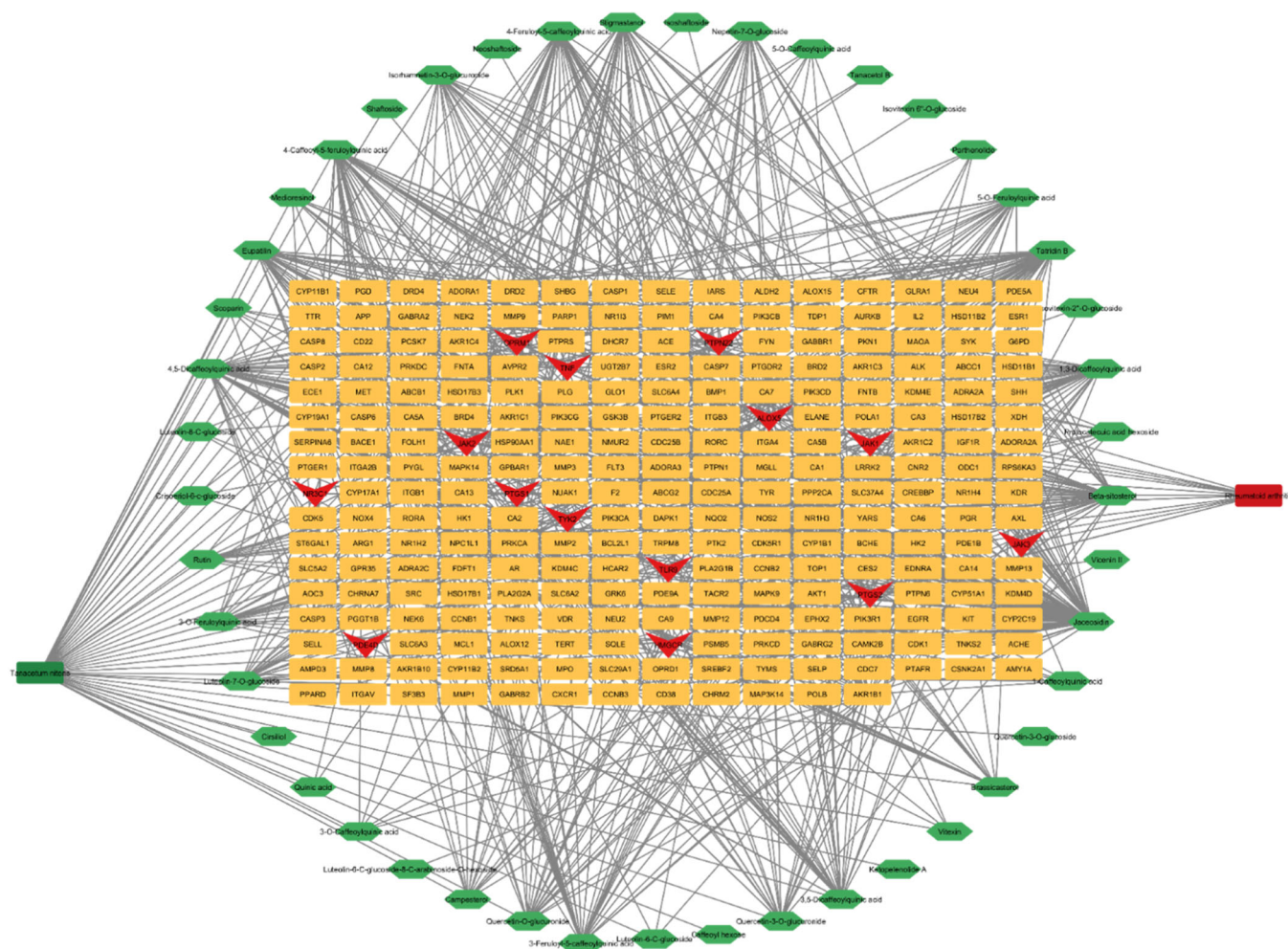
FIGURE 6 In the compound-target network of *Tanacetum nitens*, compounds are denoted by green nodes in a circular layout, while targets are represented by yellow nodes arranged in a grid layout. Nodes colored in red signify the common targets shared between *Tanacetum nitens* and rheumatoid arthritis (RA).

and subsequent activation of STAT proteins. Activated STATs then move into the nucleus, where they modulate gene expression.[61] Tofacitinib, baricitinib, upadacitinib, and filgotinib are JAK inhibitors utilized in rheumatoid arthritis treatment, with tofacitinib being a small molecule inhibitor approved by the US Food and Drug Administration (FDA) for RA therapy due to its selectivity for JAK2/JAK3.[62] The plant compound Tatridin B was predicted to bind to JAK family proteins, potentially inhibiting them and preventing the pathogenesis of RA.

2.9 | ADME profiling

The physicochemical and pharmacokinetic characteristics of *T. nitens* compounds were systematically evaluated, with supplementary data detailing the absorbtion distribution metabolism and excretion (ADME) properties of 45 compounds. Among these compounds, Cirsiliol, Eupatilin, Jaceosidin, Ketopelenolide A, Medioresinol, Parthenolide, Quinic acid, Tanacetol B, and Tatridin B demonstrated a bioavailability score of 0.55

with no Lipinski rule violations (Figure 10). Specifically, Tatridin B was forecasted to demonstrate notable gastrointestinal absorption and the potential to traverse the blood–brain barrier.

3 | CONCLUSION

To the best of our knowledge, this is the first report assessing the chemical constituents and biological activity of *T. nitens*. It was observed that the type and amount of phytochemicals recovered in different extracts were variable and significant enough to impact on the antioxidant, enzyme inhibitory, and cytotoxic properties of the plant. Overall, the presence of bioactive compounds in *T. nitens* suggests its potential as a valuable resource for the development of phytopharmaceuticals aimed at treating oxidative stress-associated diseases such as diabetes, cancer, and neurological disorders. Further exploration into isolating bioactive molecules and demonstrating their mechanism of action, along with in vivo trials, is strongly advised.
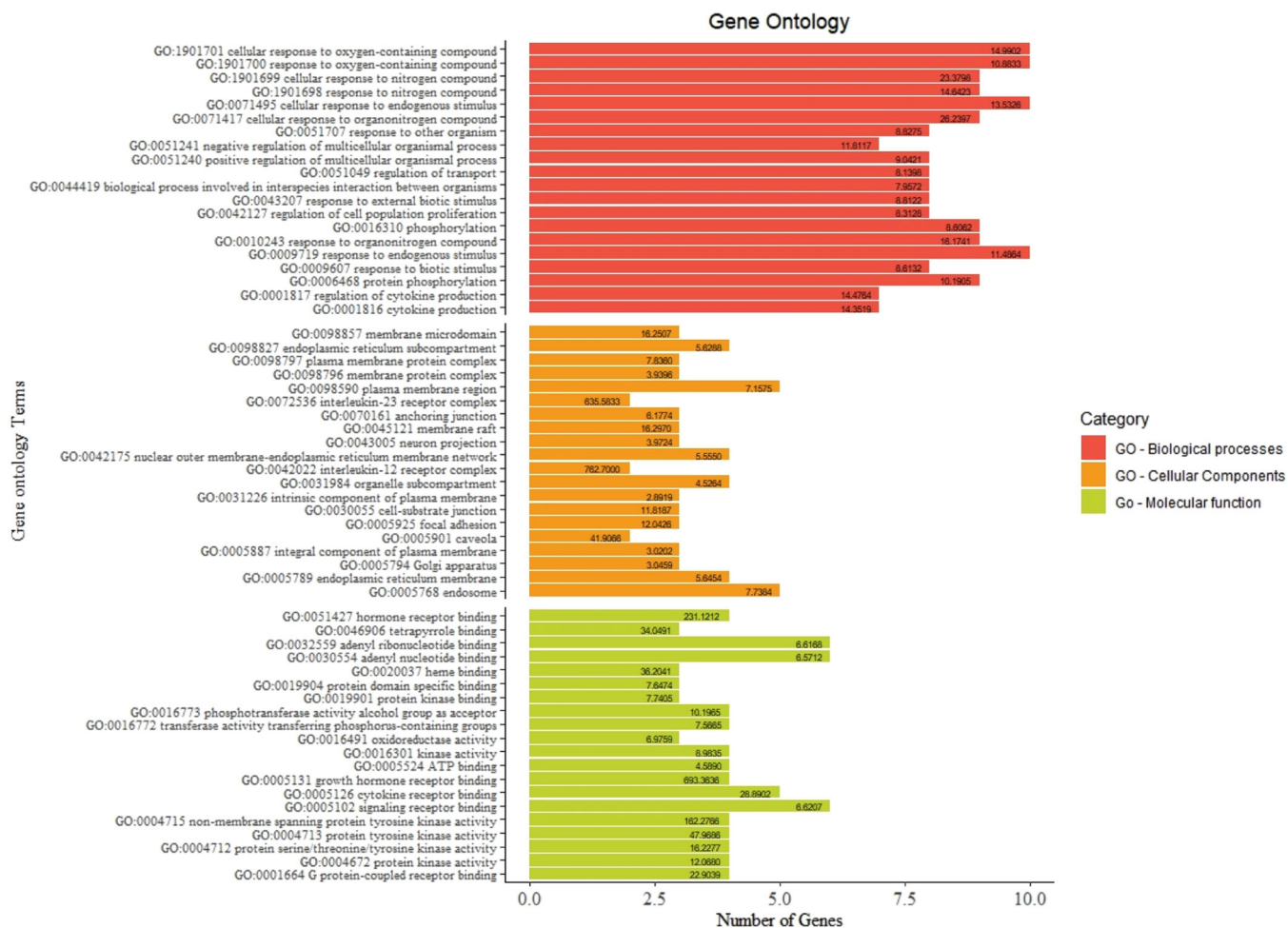
FIGURE 7 The bar plot illustrates the gene ontology of the 14 shared targets between *Tanacetum nitens* and rheumatoid arthritis (RA). Specific genes involved are indicated within the bars, corresponding to the go terms.

4 | EXPERIMENTAL

4.1 | Plant material

Plant materials were gathered from a field investigation in 2020 (Elazig, north location of Harput). Taxonomic identification, performed by Dr. Ugur Cakilcioglu, resulted in the deposition of a specimen in the herbarium of Munzur University (Voucher number: UC-20-16). Aerial parts were meticulously separated, dried in the shade at room temperature, ground into powder using a laboratory mill, and stored in darkness.

4.2 | Extraction

Four solvents, namely n-hexane, ethyl acetate, dichloromethane, methanol, and water were utilized in the preparation of extracts. Maceration of each 10 g plant material with 200 mL of n-hexane, ethyl acetate, dichloromethane, methanol, and water were carried out overnight at room temperature. Using the infusion method for

water extract, the plant material (10 g) was soaked in boiled water (200 mL) for 15 min to obtain the water extract. Subsequently, the organic solvents were evaporated for solvent removal, and the resulting water extract was dried using a freeze dryer.

4.3 | Assay for TPC and flavonoid contents

The quantification of phenols and flavonoids was conducted in accordance with the procedures outlined in the paper.[63]

4.4 | Liquid chromatography coupled with diode array and mass spectrometry, LC-HR-QTOF, LC-ESI-MS-IT, LC-APCI-QQQ

To establish the composition two different approaches were used. On one side we developed a liquid chromatography method and detection using QTOF to acquire High-resolution spectra and main fragments. Furthermore to accurately study the fragmentation of the
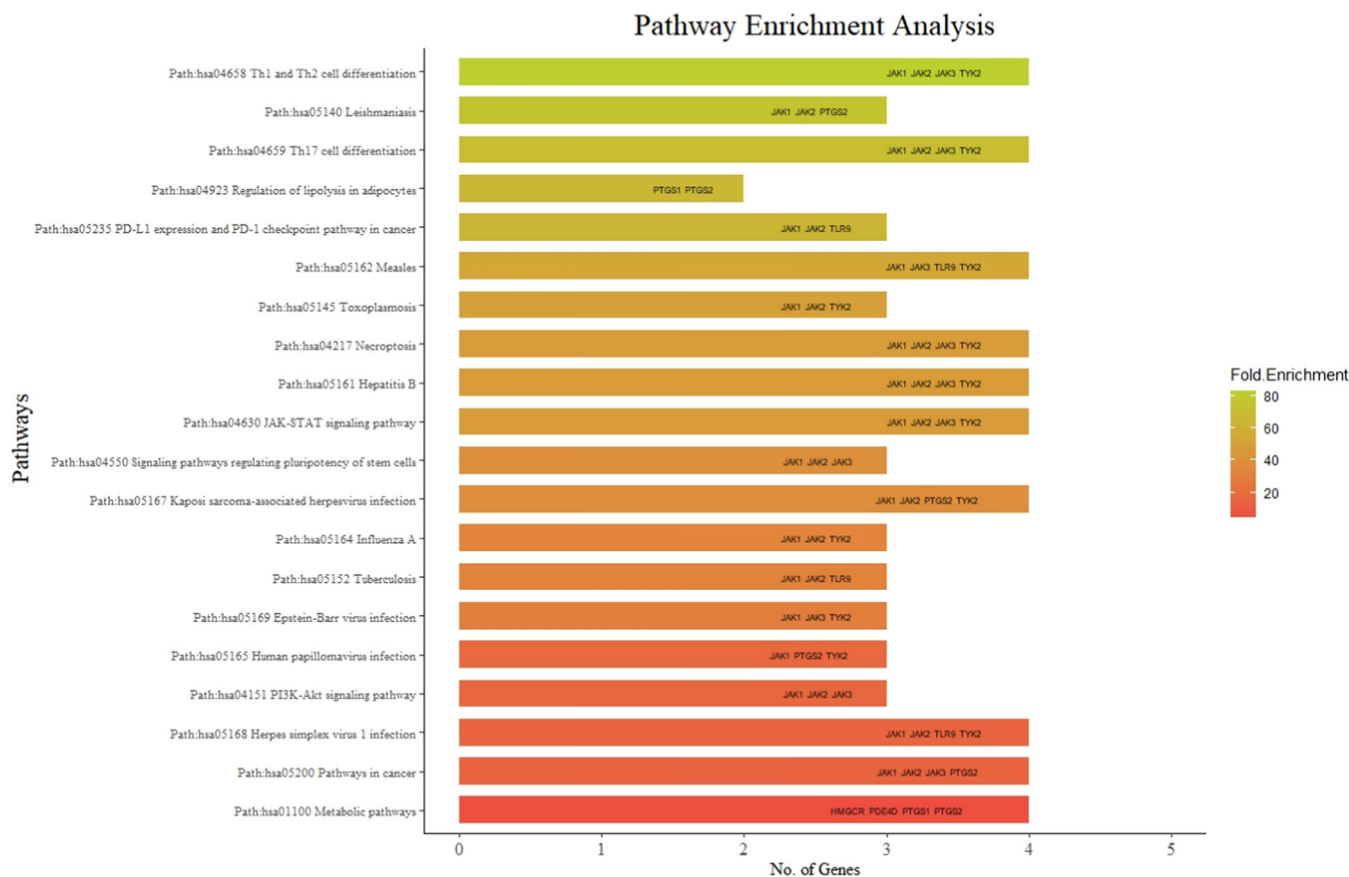
FIGURE 8 The pathway enrichment analysis for 14 common targets as bar plot representation of Kyoto Encyclopedia of Genes and Genomes (KEGG) pathways where as the color gradient represents the fold enrichment value and genes involved in the pathways were mentioned inside the bar.

detected specie, liquid chromatography coupled with ion trap (IT) allowed to obtain multiple stage mass spectrometry fragmentation. An Agilent 1290 UPLC system equipped with an autosampler and 1290 series Diode Array was used as a chromatograph coupled with the QTOF. After the column, the flow was split with a passive T junction and the liquid was sent to diode array or mass spectrometer. The Agilent 6530 QTOF was used as a detector the instrument is equipped with Jet Stream source and was operating in positive ion mode. During the acquisition, the mass were calibrated using the Agilent calibration mixture. As a stationary phase, an Agilent SB C18 (3 ×100 mm; 1.7 μm) was used. Eluents were water 0.1% formic acid (A) and acetonitrile with 0.1% formic acid (B). Flow rate was set to 0.5 mL/min. Gradient started with 90% of A remain isocratic for 1 min than go to 85% B in 10 min and then reach 90% B in 12 min and remain isocratic up to 14 min. Varian IT model MS500 equipped with ESI source was used and operated in turbodds mode acquiring MS^n spectra of eluted species. The ESI parameters were as follows needle voltage, 4600 V; capillary voltage, 80 V; RF loading, 90%; nebulizing gas pressure, 45 psi (nitrogen); drying gas pressure, 18 psi; and drying gas temperature, 295°C. The instrument's mass range extended from 50 to 2000 Da. The turbo detection data scanning (TDDS) function, with $n = 4$ levels of fragmentation, was employed to elucidate the fragmentation patterns of eluted compounds. Data of the HR and low-resolution mass spectrometry were combined to establish the identity of the eluted compounds.

For quantitative analysis catechin, epicatechin, vitexin, chlorogenic acid, parthenolide were used, calibration curves were generated preparing a solution in four concentrations namely 2, 10, 20, and 50 μg/mL and collecting chromatogram at 280 nm for flavan-3-o-ls, 350 nm for flavonoids, 254 nm for parthenolide. Vitexin, Quercetin-3-O-glucoside was used for the quantification of the flavonoids and the calibration curve was obtained using solutions obtained at 2, 10, 20, and 50 μg/mL and collecting the chromatogram at 350 nm. For the catechin and epicatechin quantification calibration curves were obtained using solutions at 5, 10, 15, and 30 μg/mL and collecting the chromatogram at 330 nm.

For the analysis of phytosterols liquid chromatography was coupled with triple quadrupole (QQQ) using Atmospheric pressude Chemical Ionization. Waters E2658 chromatograph was used, coupled with a Varian 320MS triple quadrupole equipped with an APCI ion source. As the stationary phase, an Agilent C18 XBD (3.0 × 150, mm, 3.5 μm) was used. As mobile phases, water 1% formic acid (A), acetonitrile (B), and methanol were used. Gradient start with 20% A and 70% (B) and 10% (C) in 10 min change to 90% (B) and 10% (C)
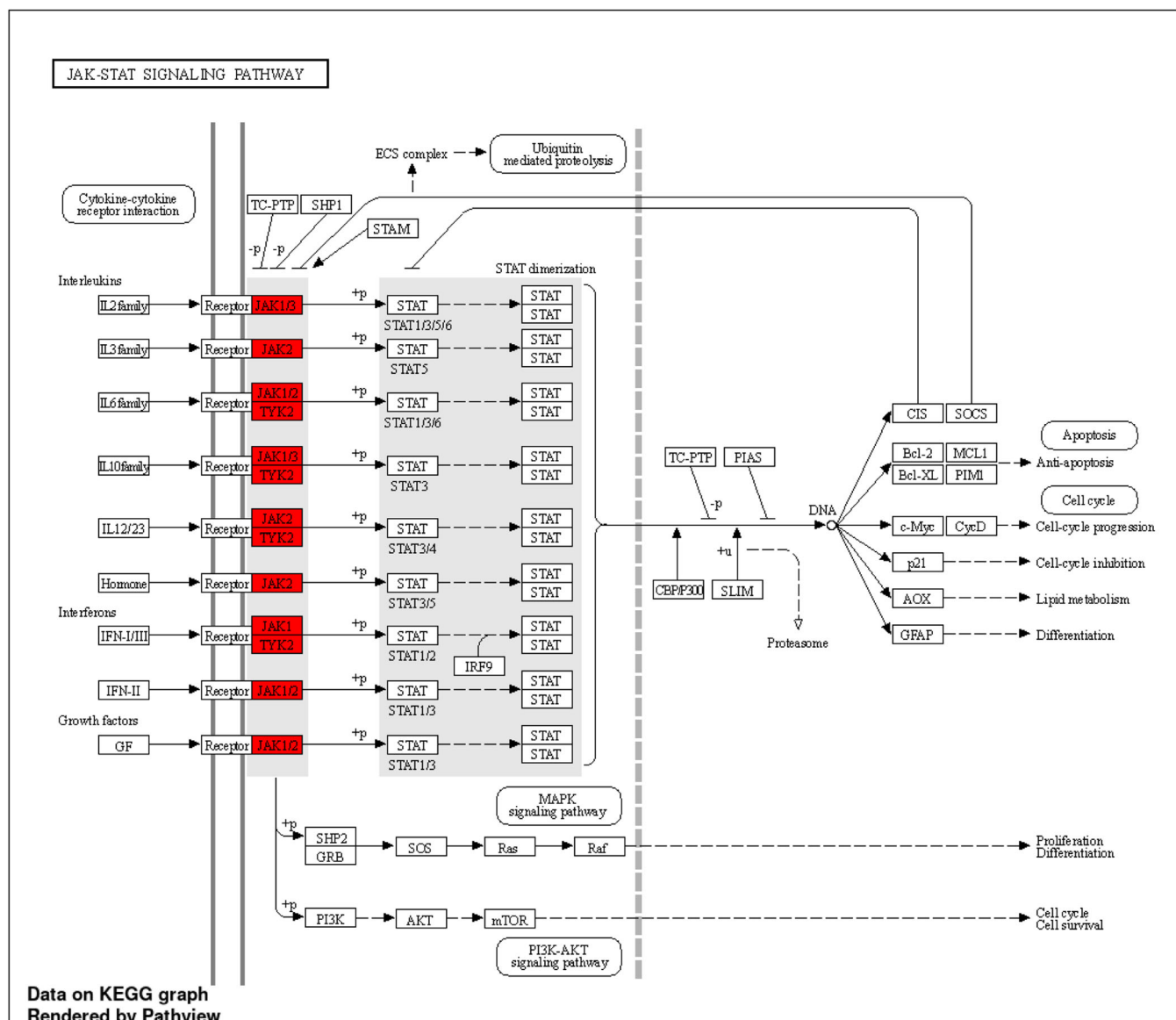
FIGURE 9 The highlighted targets were the site of action of *Tanacetum nitens* compounds in the Janus kinase/signal transducers and activators of transcription (JAK-STAT) signaling pathway.

and stay isocratic up to 33 min. Phytosterols were detected in positive mode and most of the specie are generated as $[M+H–H_2O]^+$. Method was developed starting from a previously published method (Lipids (2013) 48:949–956). In particular analyzed compounds were beta-sitosterol m/z 397→161; brassicasterol m/z 381→297; campesterol m/z 383→161; stigmasterol m/z 395→297. Reference compounds were used to prepare reference solutions and calibration curves were obtained using four levels of concentration namely 100, 50, 25, and 10 μg/mL.

4.5 | NMR

NMR experiments were obtained using a Bruker 400 MHZ spectrometer operating at 400.11 MHz for ^{1}H and 100 Mhz for ^{13}C. ^{1}H-NMR,

COSY, HMBC, HSQC-DEPT experiments were acquired using standard bruker pulses sequences optimizing values of p1, d1, and mixing times. A total of 20 mg of extracts were transferred in an Eppendorf tube, 1 mL of solvent was added (deuterated methanol or deuterated chloroform) and samples were sonicated for 10 min and centrifuged. Clear supernatants were transferred in an NMR tube.

4.6 | Antioxidant tests

In vitro antioxidant assays, based on previously reported techniques,[64] were executed. The results obtained from the DPPH, ABTS radical scavenging, CUPRAC, and FRAP tests were conveyed as milligrams of TE per gram of extract. The antioxidant potential assessed by the phosphomolybdenum (PBD) assay was measured as mmol of TE per
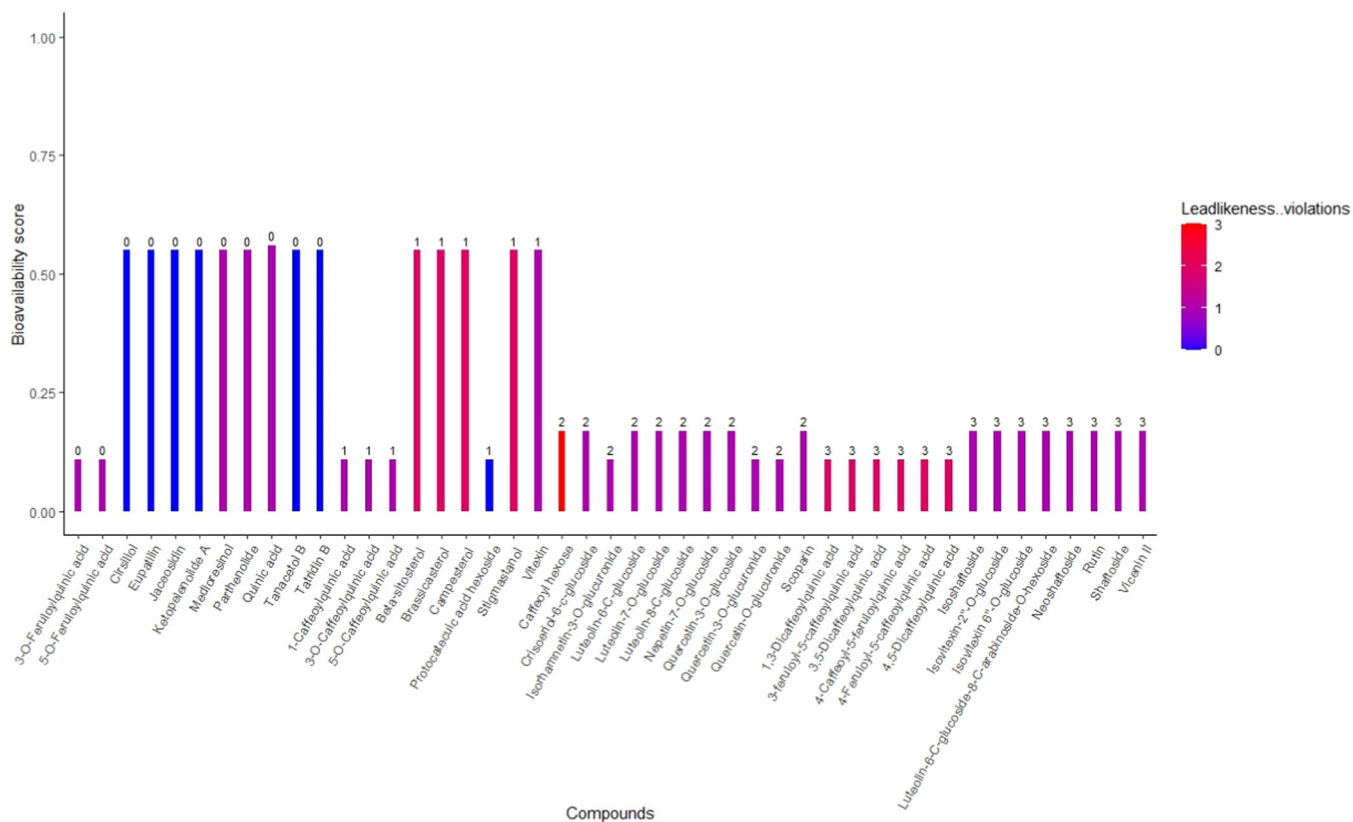
FIGURE 10 The ADME properties of the compounds are depicted in a bar plot, showcasing bioavailability and the number of Lipinski violations (numbers above the bar). The color gradient represents the lead-likeness of the compound. ADME, absorbtion distribution metabolism and excretion.

gram of extract, and metal chelating activity (MCA) was reported as milligrams of disodium edetate equivalents (EDTAE) per gram of extract.[64]

4.7 | Enzyme inhibitory tests

In accordance with established protocols, enzyme inhibition experiments were performed on the samples.[46,64] The quantification of amylase and glucosidase activity inhibition was expressed as mmol of acarbose equivalents (ACAE) per gram of extract, whereas AChE and BChE activity inhibition was denoted as milligrams of galanthamine equivalents (GALAE) per gram of extract. Tyrosinase inhibition was measured as milligrams of kojic acid equivalents (KAE) per gram of the tested extracts.

4.8 | Cell assays

4.8.1 | Cell culture

The following cancer and normal cell lines obtained from ATCC and stored in liquid nitrogen were used for the study. DU-145 (Prostate Carcinoma), MDA-MB-231 (Breast Adenocarcinoma), HELA (Cervix Adenocarcinoma), MCF-7 (Breast Adenocarcinoma), HGC-27 (Gastric

Adenocarcinoma), A549 (Lung cancer cell), and HT-29 (Colon Adenocarcinoma) cells were cultured in DMEM-F12/RPMI-1640 media supplemented with 10% fetal bovine serum (FBS), 100 μg/mL of streptomycin/100 IU/mL of penicillin in incubators at 37°C under humid conditions containing 5% CO_2.

4.8.2 | Cell viability assay

The cytotoxic effects of *T. nitens* (hexane, ethyl acetate, dicholoromethane, methanol, water, and infusiun) were assessed using the MTT (3-(4,5-dimethylthiazol-2-yl)-2,5-diphenyltetrazolium bromide) assay. The cells (DU-145, MDA-MB-231, HELA, HGC-7, A549, MCF-7, and HT-29) were incubated in the 96-well sterile plate for 24 h with 1×10^4 cells per well. The media were removed and the extracts were incubated at doses of 0, 2.5, 5, 10, 25, 50, 100, and 200 μg/mL for 24 h. A total of 10 μL of MTT (0.5 mg/mL) were added into each well as the reactive agent. After 4 h of incubation, the media was removed and substituted with 100 μL of DMSO, after which measurements were performed at OD_{570}-OD_{690}nm using a plate reader (Thermo Multiskan GO, Thermo). Following these measurements, plots were formed and IC_{50} value was calculated. The difference between the distribution of variables and normal distribution was tested by Kolmogorov–Smirnov and Shapiro–Wilk methods.

4.9 | Molecular modeling

The crystal protein complexes of AChE (PDB ID: 6O52),[65] α-amylase (PDB ID: 1B2Y),[66] BChE (PDB ID: 6EQP),[67] FGFR2 (PDB ID: 3RI1),[68] VEGFR2 (PDB ID: 4ASE),[69] and PD-L1 (PDB ID: 5N2F)[70] were retrieved from the protein data bank (https://www.rcsb.org/).[71] Furthermore, a homology model of glucosidase built using the crystal structure of glucosidase from *Mus musculus* (PDB ID: 7KBJ)[72] was retrieved from our previous study.[73] All proteins were prepared using PlayMolecule server's "ProteinPrepare module,[74] on which the predicted pKa of the titratable residues was used to protonate the proteins. Further processing was done to correct bond orders and minimize the energy of the protein structures using UCSF Chimera.[75] The three-dimensional (3D) structures of the selected bioactive compounds were downloaded from the ChEMBL database (https://www.ebi.ac.uk/chembl/) and optimized using UCSF Chimera.[75]

To prepare grid files for molecular docking, all nonpolar hydrogen atoms were merged, and Gasteiger partial charges were added to all atoms using MGLTools 1.5.6 software. A docking grid box of dimensions 50, 50, 50 Å was used and the following grid centers were applied: AChE (x: 5.0, y: 35.4, and z: 8.4 Å), BChE (x: 42.2, y: 18.0, z: 42.7 Å), tyrosinase (x: 30.0, y: 18.2, z: 96.5 Å), amylase (x: 1.5, y: 44.0, z: 22.6 Å), glucosidase (x: 13.8, y: 24.0, z: 12.4 Å). Docking was performed using AutoDock 4.2.6 (https://autodock.scripts.edu),[76] employing the Lamarckian genetic algorithm with an exhaustiveness (number of runs) of 10 for each ligand. Protein–ligand interaction was analyzed using Maestro visualizer (https://newsite.schrodinger.com/platform/products/maestro/).

4.10 | Network pharmacology

A comprehensive network pharmacology investigation was conducted on 45 compounds derived from *T. nitens* with an objective of addressing RA. The compounds' canonical SMILES were retrieved from PubChem database,[77] facilitating the compounds' targets prediction through the SwissTargetPrediction web-tool[78] and it was screened with a probability score greater than and equal to 0.1. This approach leverages the shared protein targets among structurally similar compounds. The curated targets associated with RA sourced from the Open Targets Platform were narrowed down based on an overall association score of 0.5 or higher. (https://platform.opentargets.org/disease/EFO_0000685/classic-associations). With Venny 2.1.0, common targets between *T. nitens* and RA have been identified using a Venn diagram.[79]

Using the STRING database,[80] the further analysis was conducted on the interactions among the predicted common targets, resulting in the development of a protein–protein interaction network with a minimum interaction threshold confidence level greater than 0.7. The Cytohubba tool in Cytoscape was utilized to prioritize hub genes in this network, focusing on node degree as a key criterion.

The names of common targets were subjected to gene ontology and pathway enrichment analysis using the ShinyGo 0.80 tool (http://bioinformatics.sdstate.edu/go/) tool.[81] Bar plots were employed to visually represent the top 20 gene ontology terms for biological processes, cellular components, and molecular functions, along with the top 20 KEGG pathways. Additionally, a network emphasizing KEGG pathways was created, utilizing the percentage of overlapping genes.[12,59] Additionally, the genomic locations of shared targets were extracted and displayed in a genome plot.

The physicochemical and pharmacokinetic attributes of the compounds were evaluated using Swiss ADME,[70] employing canonical SMILES representation as input. This detailed analysis offered insights into diverse physicochemical features, including hydrogen bond characteristics, molecular refractivity, lipophilicity, and water solubility. Furthermore, it delved into essential pharmacokinetic properties associated with gastrointestinal absorption, cytochrome P450 inhibition, drug-likeness, and medicinal chemistry considerations.

4.11 | Statistical analysis

In triplicate, the experiments were executed, and differences among the extracts were assessed using an analysis of variance (ANOVA) and Tukey's test. The statistical analysis was conducted using Graph Pad Prism (version 9.2).

CONFLICTS OF INTEREST STATEMENT
The authors declare no conflicts of interest.

DATA AVAILABILITY STATEMENT
The data that support the findings of this study are available from the corresponding author upon reasonable request.

ORCID
Stefano Dall'Acqua http://orcid.org/0000-0001-8264-6953
Uğur Çakılcıoğlu http://orcid.org/0000-0002-3627-3604
Gokhan Zengin http://orcid.org/0000-0001-6548-7823

REFERENCES
[1] M. C. Bergonzi, C. M. Heard, J. Garcia-Pardo, *Pharmaceutics*. **2022**, *14*, 2116.
[2] M. Yu, I. Gouvinhas, J. Rocha, A. I. R. N. A. Barros, *Sci. Rep.* **2021**, *11*(1), 10041.
[3] N. Nasim, I. S. Sandeep, S. Mohanty, *Nucleus* **2022**, *65*(3), 399.
[4] S. Khatib, M. Sobeh, C. Faraloni, L. Bouissane, *Front. Pharmacol.* **2023**, *14*, 1169629.
[5] T. Bouhlal, K. Loukili, L. Zidane, M. Fadli, *J. Med. Plants Stud.* **2017**, *5*, 170.
[6] M. Ullah, S. Mehmood, M. Ali, R. W. Bussmann, A. Aldosari, R. Ali Khan, R. Ullah, W. Hussain, M. A. Rahman Shah, *Ethnobot. Res. Appl.* **2019**, *18*, 1.
[7] M. F. Khan, A. K. Rawat, S. Khatoon, M. K. Hussain, A. Mishra, D. S. Negi, *Integr. Med. Res.* **2018**, *7*(2), 176.

[8] L. S. Godinho, L. S. Aleixo de Carvalho, C. C. Barbosa de Castro, M. M. Dias, P. F. Pinto, A. E. M. Crotti, P. L. S. Pinto, J. de Moraes, A. A. Da Silva Filho, *Sci. World J.* **2014**, *2014*, 1.

[9] N. Wszelaki, A. Kuciun, A. Kiss, *Acta Pharm.* **2010**, *60*(1), 119.

[10] H. Coté, M.-A. Boucher, A. Pichette, J. Legault, *Medicines* **2017**, *4*(2), 34.

[11] K. B. Bączek, O. Kosakowska, J. L. Przybył, E. Pióro-Jabrucka, R. Costa, L. Mondello, M. Gniewosz, A. Synowiec, Z. Węglarz, *Ind. Crops Prod.* **2017**, *102*, 154.

[12] A. Kameri, F. Koçani, Z. Hashani, K. Kurteshi, B. Kamberi, A. Kurti, A. Haziri, *Med. Sci. Monit. Basic Res.* **2019**, *25*, 179.

[13] N. Gören, N. Arda, Z. Çaliskan, *Stud. Nat. Prod. Chem.* **2002**, *27*, 547.

[14] K. Polatoğlu, H. Servi, Y. Y. Yücel, A. Nalbantsoy, *Nat. Volatiles Essent. Oils* **2015**, *2*(4), 11.

[15] F. Rezaei, R. Jamei, R. Heidari, *Pharm. Sci.* **2017**, *23*(2), 136.

[16] A. Savcı, E. Koçpınar, Y. Alan, M. Kurşat, *Int. Food Res. J.* **2020**, *27*(1), 160.

[17] E. Özmen Baysal, I. Kızılpınar, B. Ozudogru, C. Doğan, S. Erik, *Fabad J. Pharm. Sci.* **2009**, *34*(1), 1.

[18] P. H. Davis, *Flora of Turkey and the East Aegean Islands*, Edinburgh University Press, Edinburgh, UK **1970**.

[19] E. Bagci, A. Kocak, *Ind. Crops Prod.* **2010**, *31*(3), 542.

[20] R. E. K. Dibacto, B. R. T. Tchuente, M. W. Nguedjo, Y. M. T. Tientcheu, E. C. Nyobe, F. L. E. Edoun, M. F. G. Kamini, R. F. Dibanda, G. N. Medoua, *Sci. World J.* **2021**, *2021*, 1.

[21] H. Guo, K. Saravanakumar, M.-H. Wang, *Biocatal. Agric. Biotechnol.* **2018**, *15*, 235.

[22] G. Ak, R. Gevrenova, K. I. Sinan, G. Zengin, D. Zheleva, M. F. Mahomoodally, I. Senkardes, L. Brunetti, S. Leone, S. C. Di Simone, L. Recinella, A. Chiavaroli, L. Menghini, G. Orlando, C. Ferrante, *Food Chem. Toxicol.* **2021**, *153*, 112268.

[23] N. Eruygur, K. TABAN AKÇA, O. Üstün, M. Tekin, *Turk. J. Pharm. Sci.* **2022**, *19*(4), 377.

[24] R. Gevrenova, G. Zengin, K. I. Sinan, D. Zheleva-Dimitrova, V. Balabanova, M. Kolmayer, Y. Voynikov, O. Joubert, *Plants* **2022**, *12*(1), 22.

[25] S. Yur, M. Tekin, F. Göger, K. H. C. Başer, T. Özek, G. Özek, *Int. J. Food Prop.* **2017**, *20*(sup3), S2359.

[26] G. Zengin, A. Cvetanović, U. Gašić, A. Stupar, G. Bulut, I. Şenkardes, A. Dogan, K. Ibrahime Sinan, S. Uysal, Z. Aumeeruddy-Elalfi, A. Aktumsek, M. Fawzi Mahomoodally, *Ind. Crops Prod.* **2020**, *146*, 112202.

[27] C. Cravotto, A. S. Fabiano-Tixier, O. Claux, M. Abert-Vian, S. Tabasso, G. Cravotto, F. Chemat, *Foods* **2022**, *11*(21), 3412. https://doi.org/10.3390/foods11213412

[28] G. Appendino, P. Gariboldi, G. Mario Nano, *Phytochemistry* **1983**, *22*(2), 509.

[29] D. Herawati, P. E. Giriwono, F. N. A. Dewi, T. Kashiwagi, N. Andarwulan, *Int. J. Food Prop.* **2019**, *22*(1), 994.

[30] I. Atay, H. Kirmizibekmez, A. C. Gören, E. Yeşilada, *Turk. J. Chem.* **2015**, *39*(1), 34.

[31] V. Maharaj, C. C. Ezeofor, D. Naidoo Maharaj, C. J. F. Muller, N. J. Obonye, *Molecules* **2022**, *27*(22), 8095. https://doi.org/10.3390/molecules27228095

[32] L. M. D. John, W. F. Tinto, *J. Nat. Prod.* **1992**, *55*(9), 1313. https://doi.org/10.1021/np50087a022

[33] A. Raffaelli, A. Saba, *Mass Spectrom. Rev.* **2023**, *42*(4), 1152.

[34] S. Mo, L. Dong, W. J. Hurst, R. B. van Breemen, *Lipids* **2013**, *48*, 949.

[35] R. E. March, E. G. Lewars, C. J. Stadey, X.-S. Miao, X. Zhao, C. D. Metcalfe, *Int. J. Mass Spectrom.* **2006**, *248*(1–2), 61.

[36] J. Cao, C. Yin, Y. Qin, Z. Cheng, D. Chen, *J. Mass Spectrom.* **2014**, *49*(10), 1010.

[37] N. Fabre, I. Rustan, E. de Hoffmann, J. Quetin-Leclercq, *J. Am. Soc. Mass Spectrom.* **2001**, *12*(6), 707.

[38] K. Ablajan, Z. Abliz, X. Y. Shang, J. M. He, R. P. Zhang, J. G. Shi, *J. Mass Spectrom.* **2006**, *41*(3), 352.

[39] M. N. Clifford, S. Knight, N. Kuhnert, *J. Agric. Food Chem.* **2005**, *53*(10), 3821.

[40] P. J. Atria, D. Bordin, F. Marti, V. V. Nayak, J. Conejo, E. Benalcázar Jalkh, L. Witek, C. S. Sampaio, *J. Esthet. Restor. Dent.* **2022**, *34*(5), 804.

[41] N. Balasundram, K. Sundram, S. Samman, *Food Chem.* **2006**, *99*(1), 191.

[42] E. González-Molina, R. Domínguez-Perles, D. A. Moreno, C. García-Viguera, *J. Pharm. Biomed. Anal.* **2010**, *51*(2), 327.

[43] F. Babaei, A. Moafizad, Z. Darvishvand, M. Mirzababaei, H. Hosseinzadeh, M. Nassiri-Asl, *Food Sci. Nutr.* **2020**, *8*(6), 2569.

[44] Y. F. Madi, M. A. Choucry, S. A. El-Marasy, M. R. Meselhy, E.-S. A. El-Kashoury, *J. Ethnopharmacol.* **2020**, *259*, 112930.

[45] H. Sun, T. Mu, L. Xi, Z. Song, *J. Agric. Food Chem.* **2014**, *62*(36), 8982.

[46] G. Ak, G. Zengin, R. Ceylan, M. Fawzi Mahomoodally, S. Jugreet, A. Mollica, A. Stefanucci, *Flavour Fragr. J.* **2021**, *36*(5), 554. https://doi.org/10.1002/ffj.3661

[47] J. Li, H. Chang, N. Zhang, Y. He, D. Zhang, B. Liu, Y. Fang, *Talanta* **2023**, *253*, 124092.

[48] I. E. Orhan, F. Tosun, A. R. Gülpınar, M. Kartal, A. Duran, F. Mihoglugil, D. Akalgan, *Phytochem. Lett.* **2015**, *11*, 347.

[49] H. A. S. El-Nashar, M. I. G. El-Din, L. Hritcu, O. A. Eldahshan, *Molecules* **2021**, *26*(24), 7546.

[50] G. Özek, *J. Turkish Chem. Soc. Section A Chem.* **2018**, *5*(2), 493.

[51] S. Babu, M. Krishnan, P. Rajagopal, V. Periyasamy, V. Veeraraghavan, R. Govindan, S. Jayaraman, *Eur. J. Pharmacol.* **2020**, *873*, 173004.

[52] Y. M. Mandour, E. Refaat, H. D. Hassanein, *Sci. Rep.* **2023**, *13*(1), 20038.

[53] M. Sztiller-Sikorska, M. Czyz, *Pharmaceuticals* **2020**, *13*(8), 194.

[54] Zhu, S., Sun, P., Bennett, S., Charlesworth, O., Tan, R., Peng, X., Gu, Q., Kujan O., Xu J. (**2023**). *Archiv der Pharmazie 14*, 491.

[55] T. Jiang, L. Peng, Q. Wang, B. Huang, D. Peng, L. Men, Y. Jiang, M. Zhu, M. Wang, L. Lin, J. Lv, S. Li, *Cancer Cell. Int.* **2022**, *22*(1), 304.

[56] Z. Gospodinova, G. Antov, S. Angelova, M. Krasteva, *Int. J. Pharm. Sci.* **2014**, *4*, 468.

[57] S. Rosselli, M. Bruno, F. M. Raimondo, V. Spadaro, M. Varol, A. T. Koparal, A. Maggio, *Molecules* **2012**, *17*(7), 8186.

[58] B. Ivănescu, C. E. Pop, L. Vlase, A. Corciovă, D. Gherghel, G. Vochita, C. M. Teodor, *Farmacia* **2021**, *69*(1), 12.

[59] D. Kaplan, A. Ordentlich, D. Barak, N. Ariel, C. Kronman, B. Velan, A. Shafferman, *Biochemistry* **2001**, *40*(25), 7433. https://doi.org/10.1021/bi010181x

[60] S. Lushchekina, A. Nemukhin, S. Varfolomeev, P. Masson, *Chem.-Biol. Interact.* **2016**, *259*, 223. https://doi.org/10.1016/j.cbi.2016.04.007

[61] C. J. Malemud, *Ther. Adv. Musculoskelet. Dis.* **2018**, *10*(5–6), 117.

[62] B. G. Craiglow, B. A. King, *JAMA Dermatol.* **2015**, *151*(10), 1110.

[63] K. Slinkard, V. L. Singleton, *Am. J. Enol. Vitic.* **1977**, *28*(1), 49.

[64] D. M. Grochowski, S. Uysal, A. Aktumsek, S. Granica, G. Zengin, R. Ceylan, M. Locatelli, M. Tomczyk, *Phytochem. Lett.* **2017**, *20*, 365.

[65] O. Gerlits, K.-Y. Ho, X. Cheng, D. Blumenthal, P. Taylor, A. Kovalevsky, Z. Radić, *Chem.-Biol. Interact.* **2019**, *309*, 108698. https://doi.org/10.1016/j.cbi.2019.06.011

[66] R. Maurus, A. Begum, L. K. Williams, J. R. Fredriksen, R. Zhang, S. G. Withers, G. D. Brayer, *Biochemistry* **2008**, *47*(11), 3332. https://doi.org/10.1021/bi701652t

[67] T. Rosenberry, X. Brazzolotto, I. Macdonald, M. Wandhammer, M. Trovaslet-Leroy, S. Darvesh, F. Nachon, *Molecules* **2017**, *22*(12), 2098. https://doi.org/10.3390/molecules22122098

[68] S. Eathiraj, R. Palma, M. Hirschi, E. Volckova, E. Nakuci, J. Castro, C. R. Chen, T. C. K. Chan, D. S. France, M. A. Ashwell, *J. Biol. Chem.* **2011**, *286*(23), 20677. https://doi.org/10.1074/jbc.M110.213736

[69] M. McTigue, B. W. Murray, J. H. Chen, Y.-L. Deng, J. Solowiej, R. S. Kania, Molecular conformations, interactions, and properties associated with drug efficiency and clinical performance among VEGFR TK inhibitors. *Proc. Natl. Acad. Sci. USA.* **2012**, *109*(45), 18281–18289. https://doi.org/10.1073/pnas.1207759109

[70] K. Guzik, K. M. Zak, P. Grudnik, K. Magiera, B. Musielak, R. Törner, L. Skalniak, A. Dömling, G. Dubin, T. A. Holak, *J. Med. Chem.* **2017**, *60*(13), 5857. https://doi.org/10.1021/acs.jmedchem.7b00293

[71] R. G. Kurumbail, A. M. Stevens, J. K. Gierse, J. J. McDonald, R. A. Stegeman, J. Y. Pak, D. Gildehaus, J. M. iyashiro, T. D. Penning, K. Seibert, P. C. Isakson, W. C. Stallings, *Nature* **1996**, *384*(6610), 644. https://doi.org/10.1038/384644a0

[72] S. S. Karade, M. L. Hill, J. L. Kiappes, R. Manne, B. Aakula, N. Zitzmann, K. L. Warfield, A. M. Treston, R. A. Mariuzza, *J. Med. Chem.* **2021**, *64*(24), 18010. https://doi.org/10.1021/acs.jmedchem.1c01377

[73] H. A. A. Omer, G. Caprioli, D. Abouelenein, A. M. Mustafa, A. I. Uba, G. Ak, R. B. Ozturk, G. Zengin, S. Yagi, *Molecules* **2022**, *27*(17), 5590. https://doi.org/10.3390/molecules27175590

[74] G. Martínez-Rosell, T. Giorgino, G. De Fabritiis, *J. Chem. Inf. Model.* **2017**, *57*(7), 1511. https://doi.org/10.1021/acs.jcim.7b00190

[75] E. F. Pettersen, T. D. Goddard, C. C. Huang, G. S. Couch, D. M. Greenblatt, E. C. Meng, T. E. Ferrin, *J. Comput. Chem.* **2004**, *25*(13), 1605. https://doi.org/10.1002/jcc.20084

[76] G. M. Morris, R. Huey, W. Lindstrom, M. F. Sanner, R. K. Belew, D. S. Goodsell, A. J. Olson, *J. Comput. Chem.* **2009**, *30*(16), 2785. https://doi.org/10.1002/jcc.21256

[77] S. Kim, J. Chen, T. Cheng, A. Gindulyte, J. He, S. He, Q. Li, B. A. Shoemaker, P. A. Thiessen, B. Yu, L. Zaslavsky, J. Zhang, E. E. Bolton, *Nucleic Acids Res.* **2023**, *51*(D1), D1373.

[78] A. Daina, O. Michielin, V. Zoete, *Nucleic Acids Res.* **2019**, *47*(W1), W357.

[79] P. Shannon, A. Markiel, O. Ozier, N. S. Baliga, J. T. Wang, D. Ramage, N. Amin, B. Schwikowski, T. Ideker, *Genome Res.* **2003**, *13*(11), 2498.

[80] D. Szklarczyk, A. L. Gable, D. Lyon, A. Junge, S. Wyder, J. Huerta-Cepas, M. Simonovic, N. T. Doncheva, J. H. Morris, P. Bork, L. J. Jensen, C. Mering, *Nucleic Acids Res.* **2019**, *47*(D1), D607.

[81] S. X. Ge, D. Jung, R. Yao, *Bioinformatics* **2020**, *36*(8), 2628.

SUPPORTING INFORMATION

Additional supporting information can be found online in the Supporting Information section at the end of this article.